Automatica 189 (2026) 112983

Contents lists available at ScienceDirect

Automatica

journal homepage: www.elsevier.com/locate/automatica

Hierarchical optimal event-triggered framework for robust formation control of underactuated ASVs☆

Wentao Wu [a,b,c], Lei Xu [d], Ruonan Liu [a], Weidong Zhang [a,*]

[a] School of Automation and Intelligent Sensing, Shanghai Jiao Tong University, Shanghai 200240, China
[b] Department of Aeronautical and Aviation Engineering, The Hong Kong Polytechnic University, Hong Kong 999077, China
[c] Research Centre for Low-Altitude Economy, The Hong Kong Polytechnic University, Hong Kong 999077, China
[d] School of Electrical Engineering and Computer Science, KTH Royal Institute of Technology, Stockholm 100 44, Sweden

ARTICLE INFO

Article history:
Received 17 September 2024
Received in revised form 3 December 2025
Accepted 22 February 2026

Keywords:
Differential graphical game
Hierarchical formation control
Optimal event-triggered mechanism
Underactuated autonomous surface vehicles
Zero-sum game

ABSTRACT

This paper investigates a hierarchical optimal event-triggered framework for robust formation control of underactuated autonomous surface vehicles (ASVs) in the presence of external disturbances. With the game-theoretic formulations, our proposed hierarchical framework designs two optimal event-triggered mechanisms (OEMs) at both coordination and control levels to conserve communication and computational resources. Specifically, at the coordination level, a performance index is formulated to optimize both guidance velocity and maximum triggering threshold by seeking the Nash equilibrium of zero-sum game. The involved differential graphical game enables all ASVs to reach the global Nash equilibrium under OEM-based sampling schemes. At the control level, a multiple-player zero-sum game associated with the control input, sampling error, and external disturbance is constructed, and a robustness-enhanced event-triggered control law in terms of the worst-case disturbance is derived by solving the control-level Nash equilibrium. Then, an online learning implementation scheme is developed to avoid solving coupled Hamilton equations using critic neural networks. It is proven that the proposed framework not only guarantees all signals of the closed-loop system to be bounded, but also excludes Zeno behavior by ensuring the positiveness of minimum sampling intervals. Finally, simulation results are provided to validate the effectiveness of our proposed framework.

1. Introduction

The growing demand for advanced maritime operations necessitates the deployment of autonomous surface vehicles (ASVs) capable of performing coordinated missions with high reliability and efficiency (Shi et al., 2017; Shojaei, 2015). As an active research topic, formation control refers to derive a control protocol that enables a fleet of ASVs to maintain a predefined spatial distribution for specific tasks, such as oceanographic data collection and maritime security (Gu et al., 2022; Ringbäck et al., 2020). Over the past decades, various formation control approaches have been developed, including behavior-based (Balch & Arkin, 1998), virtual structure (Beard et al., 2001), leader-follower (Jin, 2016), and graph-based approaches (Wu et al., 2024).

The formation control for multiple ASVs has been extensively investigated in available works (Ihle et al., 2006; Liang et al., 2021). As stated in Peng, Wang, et al. (2021), graph-based schemes allow for the distributed implementation throughout local information interaction, thus improving the robustness, flexibility, and efficiency. Representative results include the adaptive dynamic surface control approach proposed in Peng et al. (2013), where neural networks were incorporated to handle parameter uncertainties and ocean disturbances. A curvature-unknown channel formation tracking problem was addressed in Tang et al. (2023) by developing an observer-based controller. Considering limited individual abilities of the formation system, connectivity-maintenance formation strategies were further explored based on the artificial potential functions (Gu et al., 2019) and prescribed performance functions (Dai et al., 2018; Park & Yoo, 2021). It should be noted that aforementioned methods adopt a coupling design between the formation coordination and control regulation. Such a scheme may lack the flexibility in handling diverse mission requirements. Recently, hierarchical control is gradually sparking increasing attention due to its natural advantage to decouple the group cooperation and individual regulations, with

☆ This paper is supported by the National Science and Technology Major Project under Grant 2022ZD0119900, the National Natural Science Foundation of China under Grants U2141234 and U24A20260, and Hainan Province Science and Technology Special Fund under Grant ZDYF2024GXJS003. The material in this paper was not presented at any conference. This paper was recommended for publication in revised form by Associate Editor Francesco Vasca under the direction of Editor Thomas Parisini (Control System Applications).

* Corresponding author.
E-mail addresses: wtwu95@gmail.com (W. Wu), lei5@kth.se (L. Xu), ruonan.liu@sjtu.edu.cn (R. Liu), wdzhang@sjtu.edu.cn (W. Zhang).

https://doi.org/10.1016/j.automatica.2026.112983

several results reported in literature Gao et al. (2015), Pan et al. (2024) and Wu, Peng, Liu, and Wang (2022).

The optimality of multi-ASV formation is an important yet challenging problem since it can balance the cooperation performance and control resources (Shi et al., 2023). Several optimal formation strategies have been reported in the last few years. For instance, performance indices regarding the position and yaw angle were defined in W. Wu et al. (2024) and Zhang et al. (2023), where distributed Nash equilibrium-based control laws were derived to achieve the optimal formation. Considering the unavailability of the optimal output, Wang et al. (2025) developed a distributed signal generator to reach the output optimality of all agents. In Zhao and Li (2024), a distributed model predictive contouring control method was presented to optimize both tracking accuracy and speed while penalizing the difference in contouring parameters among neighboring vehicles. In Yu et al. (2024), the Stackelberg differential graphical game was integrated into the optimal formation tracking of primary and secondary ASV subgroups. However, the implementation of aforementioned methods rely on continuous or periodic data transmissions, which inevitably lead to high computational cost and energy consumption on marine vehicles with limited onboard resources Wang et al. (2024). Therefore, a resource-efficient scheme is crucial to ensuring reliable and sustainable multi-ASV operations in the long-term maritime missions.

Event-triggered control (ETC) has garnered significant attention for reducing resource waste while preserving satisfactory control performance. The fundamental idea of ETC lies in a specific triggering condition to determine the control update or information transmission (Ding et al., 2018). Recently, many ETC results have been reported in the formation control of ASVs. In Peng, Jiang, and Wang (2021), an event-triggered enclosing formation method was introduced to reduce the data transmission of controller-to-actuator channels using threshold-fixed triggering conditions. In Zhu et al. (2022), a state-based event-triggered mechanism was designed to reduce the intermittent intervehicle communication for distributed affine formation maneuvering. Later, Xu et al. (2023) introduced an adjustable variable to design a dynamic triggering threshold for the surrounding formation control. Building on Xu et al. (2023), an improved scheme was developed in Wang et al. (2024) to further reduce the controller update by adjusting the triggering threshold and gain in parallel. Moreover, more ETC results can be found in Zhou et al. (2023), and references therein. These triggering conditions are derived based on the system stability, in which sampling instants are determined independently of performance indices. However, a larger sampling interval is generally preferable in practical implementations for resource conservation, resulting in an inherent trade-off between performance and resource (Mazo & Tabada, 2008; Zhang et al., 2022).

Recently, some researchers have begun investigating the optimality of triggering condition. In Gommans et al. (2014), an optimization-based self-triggered mechanism was develop to obtain the maximum sampling interval, but which does not affect the optimal value of cost functions. Based on the min–max strategy and the algebraic Riccati equation, Sahoo et al. (2018) developed the optimal control and sampling polices via optimizing a predefined performance index. Then, Xu et al. (2024) extended the result of Sahoo et al. (2018) to a single multiple-input nonlinear system. Nevertheless, above mentioned results are designed for a single linear system or a single nonlinear systems without external disturbances, and thus are not applicable to such a practical system of ASVs with underactuation characteristic and environmental disturbances. To the best of our knowledge, the optimality of triggering condition has rarely been investigated in hierarchical formation control.

Motivated by the above discussions, this paper presents a hierarchical optimal event-triggered formation control framework for underactuated ASVs subject to external disturbances. The main contributions of this paper are stated as follows.

(1) This paper develops a hierarchical optimal event-triggered control framework consisting of both coordination and control levels, which decouples the multi-ASV cooperation and individual regulations to enhance the flexibility and scalability. In both levels, optimal event-triggered mechanisms (OEMs) are developed to reduce the communication burden and bandwidth occupation of the control execution.
(2) At the coordination level, we define a novel performance index to simultaneously optimize both guidance velocity and its sampling interval using the zero-sum and differential graphical games. This formulation enables event-based optimal policies to be transmitted to the control level with a maximum interval and achieve the global Nash equilibrium of all players.
(3) At the control level, a robust ETC law is presented by formulating a three-player zero-sum game that unifies the control input, sampling error, and lumped disturbance. The Nash equilibrium of this game establishes optimal control and sampling policies with respect to the disturbance-worst case.
(4) This paper presents a critic learning-based implementation scheme to avoid finding the analytical solution to the coupled Hamilton equations, where the persistence of excitation condition is weakened by integrating the experience replay technique.

This paper is organized as below. Section 2 presents preliminaries and problem formulation. Section 3 designs the game-based hierarchical optimal event-triggered formation control framework. Section 4 provides a critic learning-based implementation scheme and stability analysis. Section 5 conducts the simulation illustrations. Section 6 makes the conclusion.

Notations. Let $\mathbb{N}_{>0}$ and $\mathbb{R}_{>0}$ be the sets of positive integers and nonnegative real numbers, respectively. For any $n \in \mathbb{N}_{>0}$, $\mathbf{1}_n$ and $\mathbf{0}_n$ are $n \times 1$ column vectors with all elements equal to one and zero, respectively. $\boldsymbol{I}_n$ and $\mathbf{0}_{n\times n}$ denote the $n \times n$ identity matrix and $n \times n$ matrix with all zeros. For convenience, $\mathbb{I}_{1:n}$ represents an integer set $\{1, \ldots, n\}$. Denote diag$(\cdot)$ as a block-diagonal matrix. $\lambda_{\min}(\cdot)$ and $\lambda_{\max}(\cdot)$ denote the minimum and maximum eigenvalues of a matrix, respectively.

Graph Theory: The internal information exchange of a formation system is denoted by a graph $\mathcal{G} = \{\mathcal{V}, \mathcal{E}\}$, where $\mathcal{V} = \mathbb{I}_{1:N}$ and $\mathcal{E} \subseteq \mathcal{V} \times \mathcal{V}$ are the sets of nodes and edges, respectively. For node i, $\mathcal{N}_i \triangleq \{j \in \mathcal{V} | (i, j) \in \mathcal{E}\}$ describes a set of its neighboring nodes, where the pair (i, j) being an information flow from node i to node j. $\boldsymbol{\mathcal{A}} = [a_{ij}] \in \mathbb{R}^{N\times N}$ represents the adjacency matrix with $a_{ij} > 0$ if $(i, j) \in \mathcal{E}$ and $i \neq j$, and $a_{ij} = 0$ otherwise. The Laplacian matrix of $\mathcal{G}$ is $\boldsymbol{\mathcal{L}} = [l_{ij}] \in \mathbb{R}^{N\times N}$ where $l_{ii} = \sum_{j\in\mathcal{N}_i} a_{ij}$ and $l_{ij} = -a_{ij}$ for $i \neq j$. For the formation system guided by the leader node 0, an augmented graph for all nodes is given by $\bar{\mathcal{G}} = \{\bar{\mathcal{V}}, \bar{\mathcal{E}}\}$ with $\bar{\mathcal{V}} = \mathcal{V} \cup \{0\}$. $\boldsymbol{\mathcal{A}}_0 = \text{diag}(a_{i0}) \in \mathbb{R}^{N\times N}$ is the leader matrix, where $a_{i0} > 0$ if node i can access to the leader and $a_{i0} = 0$ otherwise. For the graph $\bar{\mathcal{G}}$, the corresponding Laplacian matrix is denoted as $\bar{\boldsymbol{\mathcal{L}}} = \boldsymbol{\mathcal{L}} + \boldsymbol{\mathcal{A}}_0$.

2. Problem formulation

Consider a set of N underactuated ASVs with 3 degrees of freedom. Let (x_i, y_i) and ψ_i be position and yaw angle in the earth-fixed frame $X_E - Y_E$, and u_i, v_i, and r_i be surge, sway, and yaw

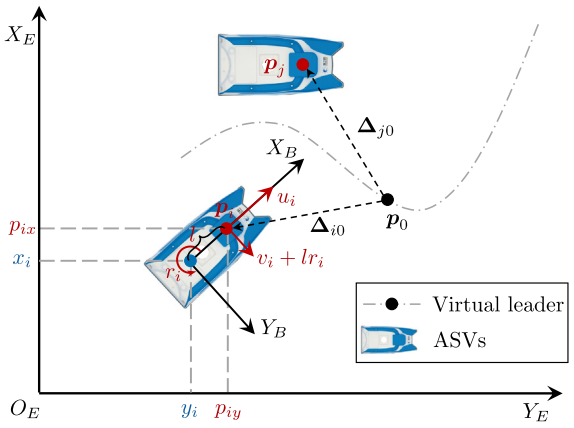

Fig. 1. Illustration for hand-position transformation.

velocities in the body-fixed frame $X_B - Y_B$. According to Fossen (2011), the mathematical model of the ASV i ($i \in \mathbb{I}_{1:N}$) subject to wind, waves, and currents can be described as

$$\begin{cases} \dot{x}_i = u_i \cos\psi_i - v_i \sin\psi_i \\ \dot{y}_i = u_i \sin\psi_i + v_i \cos\psi_i \\ \dot{\psi}_i = r_i \\ \dot{u}_i = f_{iu}(u_i, v_i, r_i) + g_{iu}\tau_{iu} + \tau_{iu}^{\omega} \\ \dot{v}_i = f_{iv}(u_i, v_i, r_i) + \tau_{iv}^{\omega} \\ \dot{r}_i = f_{ir}(u_i, v_i, r_i) + g_{ir}\tau_{ir} + \tau_{ir}^{\omega} \end{cases} \tag{1}$$

with $f_{iu}(u_i, v_i, r_i) = ((m_i - Y_{\dot{v}_i})v_i r_i + X_{u_i|u_i|}u_i|u_i| + X_{u_i}u_i)/(m_i - X_{\dot{u}_i})$, $f_{iv}(u_i, v_i, r_i) = ((-m_i + X_{\dot{u}_i})u_i r_i + Y_{v_i|v_i|}v_i|v_i| + Y_{v_i}v_i)/(m_i - Y_{\dot{v}_i})$, $f_{ir}(u_i, v_i, r_i) = ((-X_{\dot{u}_i} + Y_{\dot{v}_i})u_i v_i + N_{|r_i|r_i}r_i|r_i| + N_{r_i}r_i)/(I_{z_i} - N_{\dot{r}_i})$, $g_{iu} = 1/(m_i - X_{\dot{u}_i})$, and $g_{ir} = 1/(I_{z_i} - N_{\dot{r}_i})$ be written as $f_{iu}(\cdot)$, $f_{iv}(\cdot)$, and $f_{ir}(\cdot)$ for brevity, where m_i is the mass of the vehicle, I_{z_i} denotes the inertia moment in yaw, $\{X_{(\cdot)}, Y_{(\cdot)}, N_{(\cdot)}\}$ are hydrodynamic parameters. τ_{iu} and τ_{ir} are control force and moment, respectively. τ_{iu}^{ω} and τ_{ir}^{ω} are unknown disturbances caused by wind, waves, and currents.

Inspired by Paliotta et al. (2018), the hand-position transformation technique is employed to handle the underactuation problem of ASVs given by (1). Shown in Fig. 1, hand position refers to a point located at a predefined distance ahead of the vehicle along its surge direction. Specifically, define the coordinate transformation

$$\boldsymbol{p}_i = \begin{bmatrix} x_i + l\cos\psi_i \\ y_i + l\sin\psi_i \end{bmatrix}, \quad \boldsymbol{q}_i = \boldsymbol{R}(\psi_i)\begin{bmatrix} u_i \\ v_i + lr_i \end{bmatrix} \tag{2}$$

where $\boldsymbol{p}_i$ and $\boldsymbol{q}_i$ are states of transformed system, $l > 0$ is the hand length, which can be chosen in practice such that $\boldsymbol{p}_i$ is the position of a certain sensor on the ASV (Lu et al., 2024). $\boldsymbol{R}(\psi_i) = [\cos\psi_i, -\sin\psi_i; \sin\psi_i, \cos\psi_i]$ is the rotation matrix. Then, it yields from (2) that the dynamics of ASV i is

$$\dot{\boldsymbol{p}}_i = \boldsymbol{q}_i \tag{3}$$

$$\dot{\boldsymbol{q}}_i = \boldsymbol{\sigma}_i(\boldsymbol{q}_i) + \boldsymbol{\tau}_i + \boldsymbol{\omega}_i \tag{4}$$

with

$$\boldsymbol{\sigma}_i(\boldsymbol{q}_i) = \boldsymbol{R}(\psi_i)\begin{bmatrix} f_{iu}(\cdot) - v_i r_i - lr_i^2 \\ f_{iv}(\cdot) + lf_{ir}(\cdot) + u_i r_i \end{bmatrix},$$

$$\boldsymbol{\tau}_i = \boldsymbol{R}(\psi_i)\begin{bmatrix} g_{iu}\tau_{iu} \\ lg_{ir}\tau_{ir} \end{bmatrix}, \quad \boldsymbol{\omega}_i = \boldsymbol{R}(\psi_i)\begin{bmatrix} \tau_{iu}^{\omega} \\ \tau_{iv}^{\omega} + l\tau_{ir}^{\omega} \end{bmatrix}.$$

Remark 1. The considered dynamics (1) is a typical vehicle model equipped with only surge and yaw actuators and widely used in practice (Peng, Wang, et al., 2021). The absence of sway actuators naturally brings the underactuation property, leading to the indirect implementation of sway motion control. Recently, there have been several guidance strategies focusing on the underactuation challenge, such as line-of-sight (Wu, Peng, Wang, et al., 2022), constant bearing (Breivik et al., 2008), and pure pursuit (Breivik & Fossen, 2008). In contrast, the hand-position approach possesses two-fold advantages: (i) the modeling with hand position as system output can yield a double integrator and also remove yaw constraint; and (ii) the alignment of hand and sensor frames mitigates the deviation between measurement and desired path, thereby improving formation accuracy.

To achieve the formation mission, consider a virtual leader moving along the trajectory $\boldsymbol{p}_0 = [x_0 + l\cos\psi_0, y_0 + l\sin\psi_0]^{\top}$, where (x_0, y_0) and ψ_0 are position and angle of the leader with $\psi_0 = \text{atan2}(\dot{y}_0, \dot{x}_0)$. Then, define a distributed formation error of ASV i as

$$\begin{aligned} \boldsymbol{z}_{i1} = &\sum_{j\in\mathcal{N}_i} a_{ij}\big(\boldsymbol{p}_i - \boldsymbol{p}_j - \boldsymbol{\Delta}_{ij0}\big) \\ &+ a_{i0}\big(\boldsymbol{p}_i - \boldsymbol{p}_0 - \boldsymbol{\Delta}_{i0}\big) \end{aligned} \tag{5}$$

with $\boldsymbol{\Delta}_{ij0} = \boldsymbol{\Delta}_{i0} - \boldsymbol{\Delta}_{j0}$, where $\boldsymbol{\Delta}_{i0}$, $\boldsymbol{\Delta}_{j0} \in \mathbb{R}^2$ are the predefined deviations with respect to the leader, shown in Fig. 1.

Based on (3) and (5), the dynamics of $\boldsymbol{z}_{i1}$ is given by

$$\dot{\boldsymbol{z}}_{i1} = (d_i + a_{i0})\boldsymbol{q}_i - \sum_{j\in\mathcal{N}_i} a_{ij}\boldsymbol{q}_j - a_{i0}\dot{\boldsymbol{p}}_0 \tag{6}$$

where $d_i = \sum_{j\in\mathcal{N}_i} a_{ij}$.

Assumption 1 (*Ren & Beard, 2008*)**.** The graph $\bar{\mathcal{G}}$ contains a spanning tree with the root node being the leader node.

Assumption 2. For the leader $\boldsymbol{p}_0$, there is a constant $\bar{q}_0 > 0$ such that $\|\dot{\boldsymbol{p}}_0\| \le \bar{q}_0$.

Remark 2. Assumption 1 is a typical condition that achieves the distributed formation tracking objective. If there exist some follower ASVs that cannot directly or indirectly access the leader, they will not be capable of following the leader. Note that the matrix $\bar{\mathcal{L}}$ is asymmetric and the real parts of the eigenvalues are positive under Assumption 1. Assumption 2 is used to constrain the update rate of reference signal. From a physical perspective, bounded input energy will not generate the unrestricted change of the system output, which is mild and practical for the ASV system. Similar assumptions are adopted in the existing work, such as Peng et al. (2013), Reis et al. (2023), Ren and Beard (2008), Ye et al. (2025), and references therein.

Control Objective: This paper aims to propose a hierarchical optimal event-triggered formation control framework that can achieve: (1) each ASV can track the virtual leader and hold a predefined distance such that $\lim_{t\to\infty}\|\boldsymbol{p}_i - \boldsymbol{p}_0 - \boldsymbol{\Delta}_{i0}\| < \varepsilon_i$, where ε_i is positive constant; (2) all signals of the closed-loop system are bounded; and (3) Zeno behaviors under the designed OEMs are excluded.

3. Hierarchical optimal event-triggered formation control framework design

This section proposes a hierarchical optimal ETC framework for robust formation tracking of underactuated ASVs. In the coordination level, define a performance index involving both zero-sum game and differential graphical game to derive the optimal guidance law and sent it to the control level by the coordination-level OEM. In the control level, another performance index is

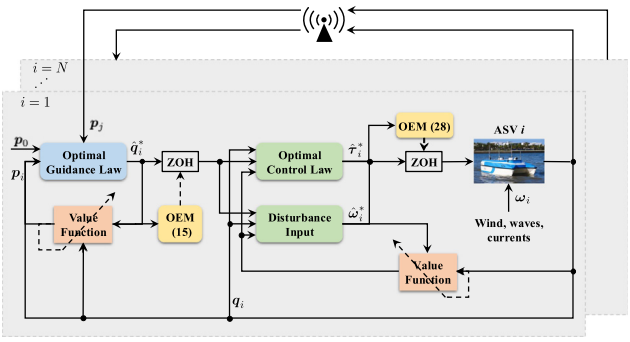

Fig. 2. Block diagram of the hierarchical optimal event-triggered formation control framework.

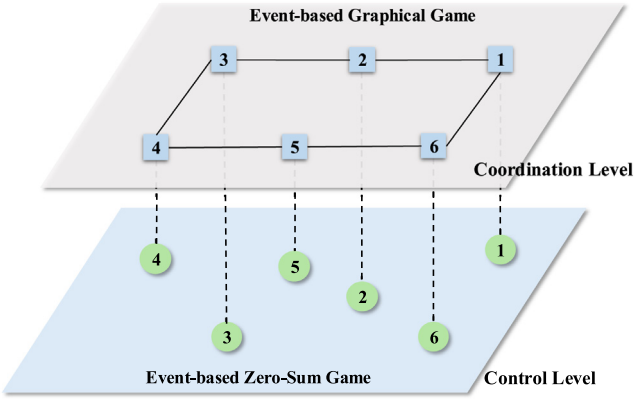

Fig. 3. Illustration on the hierarchical structure of the proposed optimal event-triggered robust formation control scheme.

presented to simultaneously optimize the control input, sampled input error, and external disturbance with a multi-player zero-sum game formulation. Then, the event-based control law and another OEM are obtained together with the worst-case disturbance. The overall diagram of developed framework is depicted in Fig. 2.

Step 1: To begin with, we denote by $\boldsymbol{p}_{i,s} = \boldsymbol{p}_i(t_{i1,s})$ and $\boldsymbol{p}_{i,s} = \boldsymbol{p}_i(t_{i1,s})$ latest states of ASV i at any instant $t_{i1,s}$, where $\{t_{i1,s}\}_{s=0}^{\infty}$ is a triggering instant sequence with $t_{i1,0} = 0$ and $s \in \mathbb{N}_{>0}$. In the framework shown in Fig. 2, neighbors of each ASV only access to the state information from it when this ASV determines to broadcast to them. Under the event-triggered implementation, we can rewrite the dynamics (6) with sampled values $\boldsymbol{q}_{i,s}$ and $\boldsymbol{q}_{j,s} = \boldsymbol{q}_j(t_{j,s})$ as

$$\dot{\boldsymbol{z}}_{i1} = (d_i + a_{i0})\boldsymbol{q}_{i,s} - \sum_{j\in\mathcal{N}_i} a_{ij}\boldsymbol{q}_{j,s} - a_{i0}\dot{\boldsymbol{p}}_0. \tag{7}$$

Let $\boldsymbol{e}_{iq,s} = \boldsymbol{q}_{i,s} - \boldsymbol{q}_i$ be the error between continuous velocity $\boldsymbol{q}_i$ and sampled velocity $\boldsymbol{q}_{i,s}$. Substituting $\boldsymbol{e}_{iq,s}$ into the dynamics (7) further yields as

$$\dot{\boldsymbol{z}}_{i1} = (d_i + a_{i0})(\boldsymbol{q}_i + \boldsymbol{e}_{iq,s}) - \sum_{j\in\mathcal{N}_i} a_{ij}\boldsymbol{q}_{j,s} - a_{i0}\dot{\boldsymbol{p}}_0. \tag{8}$$

Next, define an infinite horizon performance index for ASV i with the event-based error dynamics (8) as follows

$$J_{i1}(\boldsymbol{z}_{i1}, \boldsymbol{q}_i, \boldsymbol{e}_{iq,s}) = \int_0^{\infty} \pi_{i1}(\boldsymbol{z}_{i1}, \boldsymbol{q}_i, \boldsymbol{e}_{iq,s})dt \tag{9}$$

with $\pi_{i1}(\boldsymbol{z}_{i1}, \boldsymbol{q}_i, \boldsymbol{e}_{iq,s}) = \boldsymbol{z}_{i1}^{\top}\boldsymbol{Q}_{i1}\boldsymbol{z}_{i1} + \boldsymbol{q}_i^{\top}\boldsymbol{\Lambda}_{iq}\boldsymbol{q}_i - \gamma_{iq}^2\boldsymbol{e}_{iq,s}^{\top}\boldsymbol{e}_{iq,s}$, where $\boldsymbol{Q}_{i1} = \boldsymbol{Q}_{i1}^{\top} \in \mathbb{R}^{n\times n}$ and $\boldsymbol{\Lambda}_{iq} = \boldsymbol{\Lambda}_{iq}^{\top} \in \mathbb{R}^{m\times m}$ are positive definite matrices, and $\gamma_{iq} > 0$ is a constant satisfying $\boldsymbol{\Lambda}_{iq}^{-1} > \boldsymbol{I}_2/\gamma_{iq}^2$.

Remark 3. In the ETC scheme, the sampling interval $T_{i1,s} = t_{i1,s+1} - t_{i1,s}$ is always expected to be as long as possible to conserve communication resources, yet it may impose the negative effect on the system stability. Following this, $\boldsymbol{e}_{iq,s}$ intends to maximize the performance index (9) while the velocity $\boldsymbol{q}_i$ tries to minimize it, where the terms $\boldsymbol{q}_i$ and $\boldsymbol{e}_{iq,s}$ display the opposite objective. Thus, a min–max problem of $\boldsymbol{e}_{iq,s}$ and $\boldsymbol{q}_i$ is formulated as the zero-sum game problem. Then, minimizing (9) can simultaneously optimize $\boldsymbol{q}_i$ and $\boldsymbol{e}_{iq,s}$ to reach the Nash equilibrium. Unlike traditional ETMs in Dai et al. (2023), Huang et al. (2024) and Lu et al. (2022), this scheme establishes a bridge between sampling frequency and formation performance, which is desirable in practical implementations.

Remark 4. It is observed from (8) that the performance index J_{i1} of each ASV depends not only on its own behavior but also on the behavior of its neighbors. Then, J_{i1} can be explicitly rewritten as $J_{i1}(\boldsymbol{z}_{i1}, \boldsymbol{q}_i, \boldsymbol{e}_{iq,s}, \boldsymbol{q}_{-i}, \boldsymbol{e}_{-iq,s})$ with $\boldsymbol{q}_{-i} = [\boldsymbol{q}_1^{\top}, \ldots, \boldsymbol{q}_{i-1}^{\top}, \boldsymbol{q}_{i+1}^{\top}, \ldots, \boldsymbol{q}_N^{\top}]^{\top}$ and $\boldsymbol{e}_{-iq,s} = [\boldsymbol{e}_{1q,s}^{\top}, \ldots, \boldsymbol{e}_{(i-1)q,s}^{\top}, \boldsymbol{e}_{(i+1)q,s}^{\top}, \ldots, \boldsymbol{e}_{Nq,s}^{\top}]^{\top}$, implying that (9) involves a differential graphical game of multiple ASVs, shown in Fig. 3. This formulation provides a framework that allows each ASV to have both cooperative and competitive objectives. Herein, ASV i, $i \in \mathbb{I}_{1:N}$ tries to optimize its policy pair $(\boldsymbol{q}_i^*, \boldsymbol{e}_{iq,s}^*)$ against neighbors' policies $(\boldsymbol{q}_{-i}^*, \boldsymbol{e}_{-iq,s}^*)$ such that J_{i1} reaches to the optimal game value $J_{i1}(\boldsymbol{z}_{i1}, \boldsymbol{q}_i^*, \boldsymbol{e}_{iq,s}^*, \boldsymbol{q}_{-i}^*, \boldsymbol{e}_{-iq,s}^*)$. Therefore, the game formulation of the coordination level enables each ASV to achieve the event-based optimal outcome for the control level under the interval-maximal sampling mechanism.

To drive the convergence of system (8), define an optimal value function associated with $J_i(\boldsymbol{z}_i, \boldsymbol{u}_i, \boldsymbol{e}_{is})$ as

$$\begin{aligned} V_{i1}^*(\boldsymbol{z}_{i1}) &= \min_{\boldsymbol{q}_i}\max_{\boldsymbol{e}_{iq,s}} \int_t^{\infty} \pi_{i1}(\boldsymbol{z}_{i1}, \boldsymbol{q}_i, \boldsymbol{e}_{iq,s})d\delta \\ &= \int_t^{\infty} \pi_{i1}(\boldsymbol{z}_{i1}, \boldsymbol{q}_i^*, \boldsymbol{e}_{iq,s}^*)d\delta \end{aligned} \tag{10}$$

where $\boldsymbol{q}_i^*$ is the guidance velocity for the local control level to be updated by the corresponding OEM, $\boldsymbol{e}_{iq,s}^*$ is the maximum sampling error to be used as the triggering threshold of this OEM.

From (8) and (10), a Hamilton–Jacobi-Isaacs (HJI) equation is formulated as

$$\begin{aligned} &H_{i1}(\boldsymbol{z}_{i1}, \boldsymbol{q}_i^*, \boldsymbol{e}_{iq,s}^*, \nabla V_{i1}^*) \\ &= \pi_{i1}(\boldsymbol{z}_{i1}, \boldsymbol{q}_i^*, \boldsymbol{e}_{iq,s}^*) + \nabla V_{i1}^{*\top}\Big((d_i + a_{i0})(\boldsymbol{q}_i^* + \boldsymbol{e}_{iq,s}^*) \\ &\quad - \sum_{j\in\mathcal{N}_i} a_{ij}(\boldsymbol{q}_j^* + \boldsymbol{e}_{jq,s}^*) - a_{i0}\dot{\boldsymbol{p}}_0\Big) \end{aligned} \tag{11}$$

where $\nabla V_{i1}^* = \partial V_{i1}^*(\boldsymbol{z}_{i1})/\partial \boldsymbol{z}_{i1}$ denotes the partial derivate of $V_{i1}^*(\boldsymbol{z}_{i1})$ with respect to $\boldsymbol{z}_{i1}$.

By solving $\partial H_{i1}(\boldsymbol{z}_{i1}, \boldsymbol{q}_i^*, \boldsymbol{e}_{iq,s}^*, \nabla V_{i1}^*)/\partial \boldsymbol{q}_i = 0$ and $\partial H_{i1}(\boldsymbol{z}_{i1}, \boldsymbol{q}_i^*, \boldsymbol{e}_{iq,s}^*, \nabla V_{i1}^*)/\partial \boldsymbol{e}_{is} = 0$, the optimal strategies are obtained as

$$\boldsymbol{q}_i^* = -\frac{d_i + a_{i0}}{2}\boldsymbol{\Lambda}_{iq}^{-1}\nabla V_{i1}^*(\boldsymbol{z}_{i1}) \tag{12}$$

$$\boldsymbol{e}_{iq,s}^* = \frac{d_i + a_{i0}}{2\gamma_{iq}^2}\nabla V_{i1}^*(\boldsymbol{z}_{i1}). \tag{13}$$

Then, the event-triggered optimal guidance law for $\forall t \in [t_{i1,s}, t_{i1,s+1})$ can be given by

$$\boldsymbol{q}_{i,s}^* = -\frac{d_i + a_{i0}}{2}\boldsymbol{\Lambda}_{iq}^{-1}\nabla V_{i1}^*(\boldsymbol{z}_{i1,s}) \tag{14}$$

where $\boldsymbol{z}_{i1,s} = \sum_{j\in\mathcal{N}_i} a_{ij}(\boldsymbol{p}_{i,s} - \boldsymbol{p}_{j,s} - \boldsymbol{\Delta}_{ij0}) + a_{i0}(\boldsymbol{p}_{i,s} - \boldsymbol{p}_0 - \boldsymbol{\Delta}_{i0})$ is the sampled value of $\boldsymbol{z}_{i1}$.

To achieve the maximum-interval sampling for coordination level, we employ the optimal value $\boldsymbol{e}^*_{iq,s}$ as the triggering threshold to derive the following OEM

$$t_{i1,s+1} = \inf\left\{t > t_{i1,s} | \|\boldsymbol{e}_{iq,s}\|^2 \geq \frac{(d_i + a_{i0})^2}{4\gamma_{iq}^4}\|\nabla V^*_{i1}\|^2\right\}. \tag{15}$$

Assumption 3 (*Khalil, 2002*). For the optimal value function $V^*_{i1}(\boldsymbol{z}_{i1})$, there exists a constant $\mu_{i1} > 0$ such that $\|\nabla V^*_{i1}(\boldsymbol{z}_{i1})\| \leq \mu_{i1}\|\boldsymbol{z}_{i1}\|$.

Theorem 1. *Supposed that Assumption 3 holds and $V^*_{i1}(\boldsymbol{z}_{i1})$ satisfies the HJI equation (11), then the N-tuple policy pair $\{(\boldsymbol{q}^*_i, \boldsymbol{e}^*_{iq,s})\}_{i=1}^N$ constitutes a global Nash equilibrium, and the event-based error system (7) with the optimal guidance law (14) is asymptotically stable under the OEM (15).*

Proof. The proof is given in Appendix A.

Step 2: Based on the dynamic surface control technique, define errors $\boldsymbol{z}_{i2}$ and $\boldsymbol{z}_{iq}$ as follows

$$\boldsymbol{z}_{i2} = \boldsymbol{q}_i - \boldsymbol{\alpha}_{iq} \tag{16}$$

$$\boldsymbol{z}_{iq} = \boldsymbol{\alpha}_{iq} - \hat{\boldsymbol{q}}^*_i \tag{17}$$

where $\hat{\boldsymbol{q}}^*_i$ will be later given by (32), $\boldsymbol{\alpha}_{iq}$ is the output of the following first-order filter

$$\kappa_{i\alpha}\dot{\boldsymbol{\alpha}}_{iq} + \boldsymbol{\alpha}_{iq} = \hat{\boldsymbol{q}}^*_i, \quad \boldsymbol{\alpha}_{iq}(0) = \hat{\boldsymbol{q}}^*_i(0) \tag{18}$$

where $\kappa_{i\alpha}$ is a positive constant to be designed.

To alleviate the bandwidth load of execution channels, another event-triggered mechanism is introduced in the local control level. In this context, the control input $\boldsymbol{\tau}_{i,s} = \boldsymbol{\tau}_i(t_{i2,s})$ stored in the zero-order holder (ZOH) is released to the actuator of ASV i at the triggering instant $t_{i2,s}$ with $t_{i2,0} = 0$ and $s \in \mathbb{N}_{>0}$. Substituting the sampled input $\boldsymbol{\tau}_{i,s}$ into the dynamics of $\boldsymbol{z}_{i2}$ based on (4) and (18), then it gets

$$\dot{\boldsymbol{z}}_{i2} = \boldsymbol{\sigma}_i(\boldsymbol{q}_i) + \boldsymbol{\tau}_i + \boldsymbol{e}_{i\tau,s} + \boldsymbol{\omega}_i + \frac{\boldsymbol{z}_{iq}}{\kappa_{i\alpha}} \tag{19}$$

where $\boldsymbol{e}_{i\tau,s} = \boldsymbol{\tau}_{i,s} - \boldsymbol{\tau}_i$ is the error between the continuous control input and its sampled value.

To proceed, define an infinite horizon performance index for the event-based system (19) as follows

$$J_{i2}(\boldsymbol{z}_{i2}, \boldsymbol{\tau}_i, \boldsymbol{e}_{i\tau,s}, \boldsymbol{\omega}_i) = \int_0^\infty \pi_{i2}(\boldsymbol{z}_{i2}, \boldsymbol{\tau}_i, \boldsymbol{e}_{i\tau,s}, \boldsymbol{\omega}_i)dt \tag{20}$$

with $\pi_{i2}(\boldsymbol{z}_{i2}, \boldsymbol{\tau}_i, \boldsymbol{e}_{i\tau,s}, \boldsymbol{\omega}_i) = \boldsymbol{z}^\top_{i2}\boldsymbol{Q}_{i2}\boldsymbol{z}_{i2} + \boldsymbol{\tau}^\top_i\boldsymbol{\Lambda}_{i\tau}\boldsymbol{\tau}_i - \gamma^2_{i\tau}\boldsymbol{e}^\top_{i\tau,s}\boldsymbol{e}_{i\tau,s} - \gamma^2_{i\omega}\boldsymbol{\omega}^\top_i\boldsymbol{\omega}_i$, where $\boldsymbol{Q}_{i2} = \boldsymbol{Q}^\top_{i2} \in \mathbb{R}^{n\times n}$ and $\boldsymbol{\Lambda}_{i\tau} = \boldsymbol{\Lambda}^\top_{i\tau} \in \mathbb{R}^{m\times m}$ are positive definite matrices, $\gamma_{i\tau}$ and $\gamma_{i\omega}$ are positive constants satisfying $\gamma^2_{i\tau}\gamma^2_{i\omega}\boldsymbol{I}_2 - \gamma^2_{i\omega}\boldsymbol{\Lambda}_{i\tau} - \gamma^2_{i\tau}\boldsymbol{\Lambda}_{i\tau} > 0$.

Then, an optimal value function associated with $J_{i2}(\boldsymbol{z}_{i2}, \boldsymbol{\tau}_i, \boldsymbol{e}_{i\tau,s}, \boldsymbol{\omega}_i)$ is expressed as

$$\begin{aligned} V^*_{i2}(\boldsymbol{z}_{i2}) &= \min_{\boldsymbol{\tau}_i}\max_{\boldsymbol{e}_{i\tau,s}}\max_{\boldsymbol{\omega}_i}\int_t^\infty \pi_{i2}(\boldsymbol{z}_{i2}, \boldsymbol{\tau}_i, \boldsymbol{e}_{i\tau,s}, \boldsymbol{\omega}_i)d\delta \\ &= \int_t^\infty \pi_{i2}(\boldsymbol{z}_{i2}, \boldsymbol{\tau}^*_i, \boldsymbol{e}^*_{i\tau,s}, \boldsymbol{\omega}^*_i)d\delta \end{aligned} \tag{21}$$

where $\boldsymbol{\tau}^*_i$ is the optimal control input, $\boldsymbol{e}^*_{i\tau,s}$ is the maximum sampling error, and $\boldsymbol{\omega}^*_i$ is the worst case of external disturbances.

Based on the min–max strategy, the HJI equation associated with $V^*_{i2}(\boldsymbol{z}_{i2})$ is formulated as

$$\begin{aligned} &H_{i2}(\boldsymbol{z}_{i2}, \boldsymbol{\tau}^*_i, \boldsymbol{e}^*_{i\tau,s}, \boldsymbol{\omega}^*_i, \nabla V^*_{i2}) \\ &= \pi_{i2}(\boldsymbol{z}_{i2}, \boldsymbol{\tau}^*_i, \boldsymbol{e}^*_{i\tau,s}, \boldsymbol{\omega}^*_i) + \nabla V^{*\top}_{i2}\Big(\boldsymbol{\sigma}_i(\boldsymbol{q}_i) + \boldsymbol{\tau}^*_i \\ &\quad + \boldsymbol{e}^*_{i\tau,s} + \boldsymbol{\omega}^*_i + \frac{\boldsymbol{z}_{iq}}{\kappa_{i\alpha}}\Big) \end{aligned} \tag{22}$$

with $\nabla V^*_{i2} = \partial V^*_{i2}(\boldsymbol{z}_{i2})/\partial(\boldsymbol{z}_{i2})$.

Letting $\partial H_{i2}/\partial\boldsymbol{\tau}_i = 0$, $\partial H_{i2}/\partial\boldsymbol{e}_{i\tau,s} = 0$, and $\partial H_{i2}/\partial\boldsymbol{\omega}_i = 0$, it yields the optimal policies $\boldsymbol{\tau}^*_i$, $\boldsymbol{e}^*_{i\tau,s}$, and $\boldsymbol{\omega}^*_i$ as

$$\boldsymbol{\tau}^*_i = -\frac{1}{2}\boldsymbol{\Lambda}^{-1}_{i\tau}\nabla V^*_{i2}(\boldsymbol{z}_{i2}) \tag{23}$$

$$\boldsymbol{e}^*_{i\tau,s} = \frac{1}{2\gamma^2_{i\tau}}\nabla V^*_{i2}(\boldsymbol{z}_{i2}) \tag{24}$$

$$\boldsymbol{\omega}^*_i = \frac{1}{2\gamma^2_{i\omega}}\nabla V^*_{i2}(\boldsymbol{z}_{i2}). \tag{25}$$

Then, the event-triggered optimal control law and the optimal disturbance policy with the sampled error $\boldsymbol{z}_{i2,s} = \boldsymbol{z}_{i2}(t_{i2,s})$ are obtained as

$$\boldsymbol{\tau}^*_{i,s} = -\frac{1}{2}\boldsymbol{\Lambda}^{-1}_{i\tau}\nabla V^*_{i2}(\boldsymbol{z}_{i2,s}) \tag{26}$$

$$\boldsymbol{\omega}^*_{i,s} = \frac{1}{2\gamma^2_{i\omega}}\nabla V^*_{i2}(\boldsymbol{z}_{i2,s}) \tag{27}$$

where the next triggering instant $t_{i2,(s+1)}$ will be updated by the following OEM with $\boldsymbol{e}^*_{i\tau,s}$ being the triggering threshold

$$t_{i2,s+1} = \inf\left\{t > t_{i2,s} | \|\boldsymbol{e}_{i\tau,s}\|^2 \geq \frac{1}{4\gamma^4_{i\tau}}\|\nabla V^*_{i2}\|^2\right\}. \tag{28}$$

Remark 5. Disturbance $\boldsymbol{\omega}_i$ plays an opposite role that degrades the control performance at the control level, which demonstrates the noncooperation objective against the control input, together with the sampling error $\boldsymbol{e}_{i\tau,s}$. Then, we formulate the performance index J_{i2} as a multi-player zero-sum game problem to be optimized by minimizing $\boldsymbol{\tau}_i$ while maximizing $\boldsymbol{e}_{i\tau,s}$ and $\boldsymbol{\omega}_i$. In the game-theoretic framework, the minimization of (20) can derive the optimal values $\boldsymbol{\tau}^*_i$, $\boldsymbol{e}^*_{i\tau,s}$, and $\boldsymbol{\omega}^*_i$. The sampling strategy with $\boldsymbol{e}^*_{i\tau,s}$ as the triggering threshold can determine the maximum interval to reduce the bandwidth occupancy of the execution channel. Moreover, the worst-case disturbance $\boldsymbol{\omega}^*_i$ can achieve the minimum impact on the system performance, which is beneficial to enhance the robustness of the multi-ASV system against external disturbances.

Remark 6. Note that the implementation of above OEMs is different from the dual-trigger scheme proposed by Wu, Chen, Chadli, and Li (2024), where the trigger for speed control is forced to update once the first trigger acts. In this paper, OEMs (15) and (28) are activated and implemented at the corresponding level, which relaxes the constraint between them that allows the OEM (28) to update the controller with the lower frequency. Specifically, it gets from (13) and (15) that the smaller γ_{iq} will enlarge the triggering threshold and increase the sampling interval $T_{i1,s}$ for the coordination level. It implies that the control level holds the optimal guidance law for a longer period $T_{i1,s}$. The low update frequency from the coordination level is beneficial for converging the error $\boldsymbol{z}_{i2}$ and enlarging the control-level sampling interval $T_{i2,s} = t_{i2,s+1} - t_{i2,s}$ for a given $\gamma_{i\tau}$. In this case, the control law also holds the sampled value for a longer period, yet leads to an increase in the formation tracking error and further forces OEM in the coordination level to decrease the sampling interval $T_{i1,s}$ for better formation performance. Therefore, it shows that two OEMs indirectly influence each other's updates.

Assumption 4 (*Khalil, 2002*). For the optimal value function $V^*_{i2}(\boldsymbol{z}_{i2})$, there exists a constant $\mu_{i2} > 0$ such that $\|\nabla V^*_{i2}(\boldsymbol{z}_{i2})\| \leq \mu_{i2}\|\boldsymbol{z}_{i2}\|$.

Theorem 2. *Supposed that Assumption 4 holds and V_{i2}^* satisfies the HJI equation (22), then the policy pair $(\boldsymbol{\tau}_i^*, \boldsymbol{e}_{i\tau,s}^*, \boldsymbol{\omega}_{i,s}^*)$ constitutes the Nash equilibrium, and the event-based error system (19) with the optimal control law (23) and the worst disturbance (25) is asymptotically stable under the OEM (28).*

Proof. The proof is given in Appendix B.

4. Critic learning-based scheme for hierarchical optimal event-triggered formation

In this section, a critic learning-based scheme is presented for the hierarchical optimal event-triggered formation control of multi-ASV system, where critic NNs are used to handle unknown game values.

Step 1: Note that the implementation of aforementioned optimal strategies (12) and (13) for the coordination level depends on the associated value ∇V_{i1}^*. However, it is difficult to solve the analytical solution from HJI equation (11). To this end, we rewrite ∇V_{i1}^* based on (12) and (13) as

$$\begin{aligned}\nabla V_{i1}^* =& \frac{2\boldsymbol{\Lambda}_{iq}}{(d_i+a_{i0})^2}\Big(\kappa_{i1}\boldsymbol{z}_{i1} - \boldsymbol{\zeta}_{i1}\sum_{j\in\mathcal{N}_i} a_{ij}\boldsymbol{q}_j \\ & - a_{i0}\boldsymbol{\zeta}_{i1}\dot{\boldsymbol{p}}_0\Big) + \frac{\boldsymbol{\Lambda}_{iq}}{(d_i+a_{i0})^2}\nabla V_{i1}^0 \end{aligned} \tag{29}$$

where $\kappa_{i1} > 0$ is a constant, $\boldsymbol{\zeta}_{i1} = \gamma_{iq}^2(\gamma_{iq}^2\boldsymbol{I}_2 - \boldsymbol{\Lambda}_{iq})^{-1}$, and $\nabla V_{i1}^0 = (d_i+a_{i0})^2\boldsymbol{\Lambda}_{iq}^{-1}\nabla V_{i1}^* - 2(\kappa_{i1}\boldsymbol{z}_{i1} - \boldsymbol{\zeta}_{i1}(\sum_{j\in\mathcal{N}_i} a_{ij}\boldsymbol{q}_j + a_{i0}\dot{\boldsymbol{p}}_0))$.

Considering the unknown ∇V_{i1}^*, then the nonlinear function ∇V_{i1}^0 can be approximated by a single critic NN

$$\nabla V_{i1}^0(\boldsymbol{z}_{i1}, \boldsymbol{p}_i) = \boldsymbol{\varphi}_{i1}^\top(\boldsymbol{z}_{i1}, \boldsymbol{p}_i)\boldsymbol{\Theta}_{ic1} + \boldsymbol{\epsilon}_{ic1} \tag{30}$$

where $\boldsymbol{\varphi}_{i1}(\boldsymbol{z}_{i1}, \boldsymbol{p}_i) \in \mathbb{R}^{2m\times 2}$ is 2×2 block diagonal matrix with diagonal elements being activation functions, $\boldsymbol{\Theta}_{ic1} \in \mathbb{R}^{2m}$ and $\boldsymbol{\epsilon}_{ic1} \in \mathbb{R}^2$ denote the ideal weight and approximation error bounded by $\|\boldsymbol{\Theta}_{ic1}\| \le \bar{\theta}_{ic1} \in \mathbb{R}^+$ and $\|\boldsymbol{\epsilon}_{ic1}\| \le \bar{\epsilon}_{ic1} \in \mathbb{R}^+$, respectively.

Since the ideal weight $\boldsymbol{\Theta}_{ic1}$ is unknown, the function ∇V_{i1}^0 can be replaced by its estimation $\nabla\hat{V}_{i1}^0 = \boldsymbol{\varphi}_{i1}^\top(\boldsymbol{z}_{i1}, \boldsymbol{p}_i)\hat{\boldsymbol{\Theta}}_{ic1}$ with $\hat{\boldsymbol{\Theta}}_{ic1}$ being the estimation of $\boldsymbol{\Theta}_{ic1}$. Then, it yields that estimations of ∇V_{i1}^*, $\boldsymbol{q}_i^*$, and $\boldsymbol{e}_{iq,s}^*$ by incorporating $\nabla\hat{V}_{i1}^0$

$$\begin{aligned}\nabla\hat{V}_{i1}^* =& \frac{2\boldsymbol{\Lambda}_{iq}}{(d_i+a_{i0})^2}\Big(\kappa_{i1}\boldsymbol{z}_{i1} - \boldsymbol{\zeta}_{i1}\sum_{j\in\mathcal{N}_i} a_{ij}\boldsymbol{q}_j \\ & - a_{i0}\boldsymbol{\zeta}_{i1}\dot{\boldsymbol{p}}_0 + \frac{1}{2}\boldsymbol{\varphi}_{i1}^\top(\boldsymbol{z}_{i1}, \boldsymbol{p}_i)\hat{\boldsymbol{\Theta}}_{ic1}\Big) \end{aligned} \tag{31}$$

$$\begin{aligned}\hat{\boldsymbol{q}}_i^* =& -\frac{1}{d_i+a_{i0}}\Big(\kappa_{i1}\boldsymbol{z}_{i1} - \boldsymbol{\zeta}_{i1}\sum_{j\in\mathcal{N}_i} a_{ij}\boldsymbol{q}_j \\ & - a_{i0}\boldsymbol{\zeta}_{i1}\dot{\boldsymbol{p}}_0 + \frac{1}{2}\boldsymbol{\varphi}_{i1}^\top(\boldsymbol{z}_{i1}, \boldsymbol{p}_i)\hat{\boldsymbol{\Theta}}_{ic1}\Big) \end{aligned} \tag{32}$$

$$\begin{aligned}\hat{\boldsymbol{e}}_{iq,s}^* =& \frac{\boldsymbol{\Lambda}_{iq}}{\gamma_{iq}^2(d_i+a_{i0})}\Big(\kappa_{i1}\boldsymbol{z}_{i1} - \boldsymbol{\zeta}_{i1}\sum_{j\in\mathcal{N}_i} a_{ij}\boldsymbol{q}_j \\ & - a_{i0}\boldsymbol{\zeta}_{i1}\dot{\boldsymbol{p}}_0 + \frac{1}{2}\boldsymbol{\varphi}_{i1}^\top(\boldsymbol{z}_{i1}, \boldsymbol{p}_i)\hat{\boldsymbol{\Theta}}_{ic1}\Big). \end{aligned} \tag{33}$$

To proceed, the associated HJI from (11) is derived as

$$\begin{aligned}&\hat{H}_{i1}(\boldsymbol{z}_{i1}, \hat{\boldsymbol{q}}_i^*, \hat{\boldsymbol{e}}_{iq,s}^*, \nabla\hat{V}_{i1}^*) \\ &= \pi_{i1}(\boldsymbol{z}_{i1}, \hat{\boldsymbol{q}}_i^*, \hat{\boldsymbol{e}}_{iq,s}^*) + \nabla\hat{V}_{i1}^{*\top}\Big((d_i+a_{i0})(\hat{\boldsymbol{q}}_i^* + \hat{\boldsymbol{e}}_{iq,s}^*) \\ &\quad - \sum_{j\in\mathcal{N}_i} a_{ij}(\hat{\boldsymbol{q}}_j^* + \hat{\boldsymbol{e}}_{jq,s}^*) - a_{i0}\dot{\boldsymbol{p}}_0\Big) \triangleq e_{ic1} \end{aligned} \tag{34}$$

where e_{ic1} denotes the Bellman residual error. To minimize the square function $E_{ic1} = e_{ic1}^2/2$, an adaptive law is designed to tune the NN weight given by

$$\dot{\hat{\boldsymbol{\Theta}}}_{ic1} = -\frac{\eta_{i1}\boldsymbol{\chi}_{i1}}{b_{i1}^2}e_{ic1} - \sum_{\ell=1}^{N_\ell}\frac{\eta_{i1}\boldsymbol{\chi}_{i1,\ell}}{b_{i1,\ell}^2}e_{ic1,\ell} \tag{35}$$

where $\eta_{i1} > 0$ is a constant, and $b_{i1} = 1 + \boldsymbol{\chi}_{i1}^\top\boldsymbol{\chi}_{i1}$ with $\boldsymbol{\chi}_{i1} = \partial e_{ic1}/\partial\hat{\boldsymbol{\Theta}}_{ic1} = \boldsymbol{\varphi}_{i1}\boldsymbol{\Lambda}_{iq}((d_i+a_{i0})(\hat{\boldsymbol{q}}_i^* + \hat{\boldsymbol{e}}_{iq,s}^*) - \sum_{j\in\mathcal{N}_i} a_{ij}(\boldsymbol{q}_j^* + \boldsymbol{e}_{jq,s}^*) - a_{i0}\dot{\boldsymbol{p}}_0)/(d_i+a_{i0})^2$. The last term integrates the experience replay technique (Chowdhary & Johnson, 2010) to relax the persistency of excitation condition. $\boldsymbol{\chi}_{i1,\ell}$, $e_{ic1,\ell}$, and $b_{i1,\ell}$ are the stored historical data over $t_\ell \in [t_{i1,s}, t_{i1,(s+1)})$ for $\ell \in \{1, 2, \ldots, N_\ell\}$ with $N_\ell > 1$ being the number of NN nodes.

Step 2: Similar to the reconstruction of (29), then decompose ∇V_{i2}^* as

$$\begin{aligned}\nabla V_{i2}^* =& 2\boldsymbol{\Lambda}_{i\tau}\Big(\kappa_{i2}\boldsymbol{z}_{i2} + \boldsymbol{\zeta}_{i2}\boldsymbol{\sigma}_i(\boldsymbol{q}_i) + \frac{1}{\kappa_{i\alpha}}\boldsymbol{\zeta}_{i2}\boldsymbol{z}_{iq}\Big) \\ & + \boldsymbol{\Lambda}_{i\tau}\nabla V_{i2}^0 \end{aligned} \tag{36}$$

where $\kappa_{i2} > 0$ is a constant, $\boldsymbol{\zeta}_{i2} = \gamma_{i\tau}^2\gamma_{i\omega}^2(\gamma_{i\tau}^2\gamma_{i\omega}^2\boldsymbol{I}_2 - \gamma_{i\omega}^2\boldsymbol{\Lambda}_{i\tau} - \gamma_{i\tau}^2\boldsymbol{\Lambda}_{i\tau})^{-1}$ and $\nabla V_{i2}^0 = \boldsymbol{\Lambda}_{i\tau}^{-1}\nabla V_{i2}^* - 2\kappa_{i2}\boldsymbol{z}_{i2} - 2\boldsymbol{\zeta}_{i2}(\boldsymbol{\sigma}_i(\boldsymbol{q}_i) + \boldsymbol{z}_{iq}/\kappa_{i\alpha})$.

It is noted that smooth functions $\boldsymbol{\sigma}_i(\boldsymbol{q}_i)$ and ∇V_{i2}^0 are unknown, thus there exist NNs $\boldsymbol{\varphi}_{i\sigma}^\top(\boldsymbol{q}_i)\boldsymbol{\Theta}_{i\sigma}$ and $\boldsymbol{\varphi}_{i2}^\top(\boldsymbol{z}_{i2}, \boldsymbol{q}_i)\boldsymbol{\Theta}_{ic2}$ such that

$$\boldsymbol{\sigma}_i(\boldsymbol{q}_i) = \boldsymbol{\varphi}_{i\sigma}^\top(\boldsymbol{q}_i)\boldsymbol{\Theta}_{i\sigma} + \boldsymbol{\epsilon}_{i\sigma} \tag{37}$$

$$\nabla V_{i2}^0(\boldsymbol{z}_{i2}, \boldsymbol{q}_i) = \boldsymbol{\varphi}_{i2}^\top(\boldsymbol{z}_{i2}, \boldsymbol{q}_i)\boldsymbol{\Theta}_{ic2} + \boldsymbol{\epsilon}_{ic2} \tag{38}$$

where $\boldsymbol{\varphi}_{i\sigma}(\boldsymbol{q}_i) \in \mathbb{R}^{2m\times 2}$ and $\boldsymbol{\varphi}_{i2}(\boldsymbol{z}_{i2}, \boldsymbol{q}_i) \in \mathbb{R}^{2m\times 2}$ are activation functions, $\boldsymbol{\Theta}_{i\sigma} \in \mathbb{R}^{2m}$ and $\boldsymbol{\Theta}_{i2} \in \mathbb{R}^{2m}$ are ideal NN weights bounded by $\|\boldsymbol{\Theta}_{i\sigma}\| \le \bar{\theta}_{i\sigma} \in \mathbb{R}^+$ and $\|\boldsymbol{\Theta}_{ic2}\| \le \bar{\theta}_{ic2} \in \mathbb{R}^+$, and $\boldsymbol{\epsilon}_{i\sigma} \in \mathbb{R}^2$ and $\boldsymbol{\epsilon}_{ic2} \in \mathbb{R}^2$ represent approximation errors with $\|\boldsymbol{\epsilon}_{i\sigma}\| \le \bar{\epsilon}_{i\sigma} \in \mathbb{R}^+$ and $\|\boldsymbol{\epsilon}_{ic2}\| \le \bar{\epsilon}_{ic2} \in \mathbb{R}^+$.

Based on optimal policies (23)–(25), then yield approximated values of ∇V_{i2}^*, $\boldsymbol{\tau}_i^*$, $\boldsymbol{e}_{i\tau,s}^*$, and $\boldsymbol{\omega}_i^*$ as

$$\begin{aligned}\nabla\hat{V}_{i2}^* =& 2\boldsymbol{\Lambda}_{i\tau}\Big(\kappa_{i2}\boldsymbol{z}_{i2} + \boldsymbol{\zeta}_{i2}\boldsymbol{\varphi}_{i\sigma}^\top(\boldsymbol{q}_i)\hat{\boldsymbol{\Theta}}_{i\sigma} + \frac{1}{\kappa_{i\alpha}}\boldsymbol{\zeta}_{i2}\boldsymbol{z}_{iq} \\ & + \frac{1}{2}\boldsymbol{\varphi}_{i2}^\top(\boldsymbol{z}_{i2}, \boldsymbol{q}_i)\hat{\boldsymbol{\Theta}}_{ic2}\Big) \end{aligned} \tag{39}$$

$$\begin{aligned}\hat{\boldsymbol{\tau}}_i^* =& -\kappa_{i2}\boldsymbol{z}_{i2} - \boldsymbol{\zeta}_{i2}\boldsymbol{\varphi}_{i\sigma}^\top(\boldsymbol{q}_i)\hat{\boldsymbol{\Theta}}_{i\sigma} - \frac{1}{\kappa_{i\alpha}}\boldsymbol{\zeta}_{i2}\boldsymbol{z}_{iq} \\ & - \frac{1}{2}\boldsymbol{\varphi}_{i2}^\top(\boldsymbol{z}_{i2}, \boldsymbol{q}_i)\hat{\boldsymbol{\Theta}}_{ic2} \end{aligned} \tag{40}$$

$$\begin{aligned}\hat{\boldsymbol{e}}_{i\tau,s}^* =& \frac{\boldsymbol{\Lambda}_{i\tau}}{\gamma_{i\tau}^2}\Big(\kappa_{i2}\boldsymbol{z}_{i2} + \boldsymbol{\zeta}_{i2}\boldsymbol{\varphi}_{i\sigma}^\top(\boldsymbol{q}_i)\hat{\boldsymbol{\Theta}}_{i\sigma} + \frac{1}{\kappa_{i\alpha}}\boldsymbol{\zeta}_{i2}\boldsymbol{z}_{iq} \\ & + \frac{1}{2}\boldsymbol{\varphi}_{i2}^\top(\boldsymbol{z}_{i2}, \boldsymbol{q}_i)\hat{\boldsymbol{\Theta}}_{ic2}\Big) \end{aligned} \tag{41}$$

$$\begin{aligned}\hat{\boldsymbol{\omega}}_i^* =& \frac{\boldsymbol{\Lambda}_{i\tau}}{\gamma_{i\omega}^2}\Big(\kappa_{i2}\boldsymbol{z}_{i2} + \boldsymbol{\zeta}_{i2}\boldsymbol{\varphi}_{i\sigma}^\top(\boldsymbol{q}_i)\hat{\boldsymbol{\Theta}}_{i\sigma} + \frac{1}{\kappa_{i\alpha}}\boldsymbol{\zeta}_{i2}\boldsymbol{z}_{iq} \\ & + \frac{1}{2}\boldsymbol{\varphi}_{i2}^\top(\boldsymbol{z}_{i2}, \boldsymbol{q}_i)\hat{\boldsymbol{\Theta}}_{ic2}\Big). \end{aligned} \tag{42}$$

where $\boldsymbol{\varphi}_{i\sigma}^\top(\boldsymbol{q}_i)\hat{\boldsymbol{\Theta}}_{i\sigma}$ and $\boldsymbol{\varphi}_{i2}^\top(\boldsymbol{z}_{i2}, \boldsymbol{q}_i)\hat{\boldsymbol{\Theta}}_{ic2}$ are the outputs of the identifier (37) and critic NN (38) with $\hat{\boldsymbol{\Theta}}_{i\sigma}$ and $\hat{\boldsymbol{\Theta}}_{ic2}$ being estimations of $\boldsymbol{\Theta}_{i\sigma}$ and $\boldsymbol{\Theta}_{ic2}$.

With the gradient descent and experience replay techniques, the adaptive laws are developed to update weights as

$$\dot{\hat{\boldsymbol{\Theta}}}_{ic2} = -\frac{\eta_{i2}\boldsymbol{\chi}_{i2}}{b_{i2}^2}e_{ic2} - \sum_{\ell=1}^{N_\ell}\frac{\eta_{i2}\boldsymbol{\chi}_{i2,\ell}}{b_{i2,\ell}^2}e_{ic2,\ell} \tag{43}$$

$$\dot{\hat{\boldsymbol{\Theta}}}_{i\sigma} = \Gamma_i(\boldsymbol{\varphi}_{i\sigma}\boldsymbol{z}_{i2} - \eta_{i3}\hat{\boldsymbol{\Theta}}_{i\sigma}) \tag{44}$$

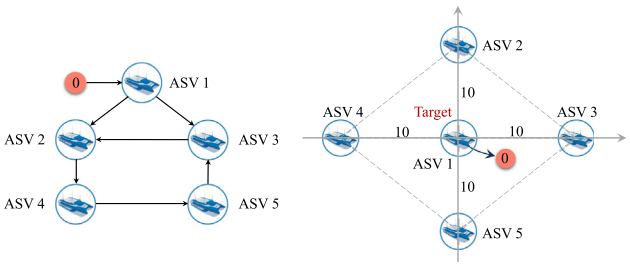

Fig. 4. The communication topology and the predefined formation for follower ASVs and virtual leader.

Table 1
Model parameters of ASVs used in simulation.

Parameter	Value	Parameter	Value
m_i	23.8	I_{z_i}	1.76
X_{u_i}	−0.7225	$X_{\dot{u}_i}$	2.0
$X_{u_i\|u_i\|}$	−1.3274	Y_{v_i}	−0.8612
$Y_{\dot{v}_i}$	−10	$Y_{v_i\|v_i\|}$	−36.2823
N_{r_i}	−1.9	$N_{\dot{r}_i}$	−1
$N_{\|r_i\|r_i}$	−0.75		

where $\eta_{i2} > 0$, $\eta_{i3} > 0$, and $\Gamma_i > 0$ are the designed constants, $e_{ic2} \triangleq \pi_{i2}(\boldsymbol{z}_{i2}, \hat{\boldsymbol{\tau}}_i^*, \hat{\boldsymbol{e}}_{i\tau,s}^*, \hat{\boldsymbol{\omega}}_i^*) + \nabla \hat{V}_{i2}^{*\top}(\boldsymbol{\varphi}_{i\sigma}^\top(\boldsymbol{q}_i)\hat{\boldsymbol{\Theta}}_{i\sigma} + \hat{\boldsymbol{\tau}}_i^* + \hat{\boldsymbol{e}}_{i\tau,s}^* + \hat{\boldsymbol{\omega}}_i^* + \boldsymbol{z}_{iq}/\kappa_{i\alpha})$, $b_{i2} = 1 + \boldsymbol{\chi}_{i2}^\top \boldsymbol{\chi}_{i2}$ with $\boldsymbol{\chi}_{i2} = \partial e_{ic2}/\partial \hat{\boldsymbol{\Theta}}_{ic2} = \boldsymbol{\varphi}_{i2}\boldsymbol{\Lambda}_{i\tau}(\hat{\boldsymbol{\Theta}}_{i\sigma}^\top \boldsymbol{\varphi}_{i\sigma}(\boldsymbol{q}_i) + \hat{\boldsymbol{\tau}}_i^* + \hat{\boldsymbol{e}}_{i\tau,s}^* + \hat{\boldsymbol{\omega}}_i^* + \boldsymbol{z}_{iq}/\kappa_{i\alpha})$, and $\boldsymbol{\chi}_{i2,\ell}$, $e_{ic2,\ell}$, $b_{i2,\ell}$ represent stored values of $\boldsymbol{\chi}_{i2}$, e_{ic2} and b_{i2} at ℓth recorded instant.

Theorem 3. *Consider underactuated ASVs with dynamics (1), the critic learning-based policies (32), (33), and (40)–(42), the first-order filter (18), and the adaptive laws (35), (43), and (44). Under Assumptions 1–2, then i) all error signals of the resulting closed-loop system are bounded, namely all ASVs achieve the predefined formation with given deviations; and ii) Zeno behavior is excluded by ensuing the positive minimum sampling interval* $T_{ik,\min} = \lambda_{\min}(\boldsymbol{\zeta}_{ik})\ln(\Psi_{ik,\min}+1)/\kappa_{ik} > 0$, $k = 1, 2$, *where* $\Psi_{ik,\min}$ *is a positive constant.*

Proof. The proof is given in Appendix C.

5. Simulation results

This section provides a simulation case to validate the effectiveness of our proposed method. Consider a 5-ASV formation control for target tracking problem, where ASV 1 acts as an evader and ASVs 2–5 act as pursuers. The communication topology among ASVs and virtual leader is displayed in Fig. 4, which also depicts the desired spatial configuration with predefined deviations $\boldsymbol{\Delta}_{10} = [0, 0]^\top$, $\boldsymbol{\Delta}_{20} = [0, 10]^\top$, $\boldsymbol{\Delta}_{30} = [10, 0]^\top$, $\boldsymbol{\Delta}_{40} = [-10, 0]^\top$, and $\boldsymbol{\Delta}_{50} = [0, -10]^\top$. In this scenario, ASV 1 is guided by a virtual leader (labeled as 0) to follow a given trajectory $[x_0(t), y_0(t)]^\top = [40 - 40\sqrt{2}\sin(t/80 + 3\pi/16), 40 - 40\sqrt{2}\cos(t/80 + 3\pi/16)]^\top$. In the simulation, model parameters of used ASVs are presented in Table 1 for brevity. And initial states of the evading ASV together with follower ASVs are set as $[20, -10, \pi/2]^\top$, $[30, -10, \pi/2]^\top$, $[40, -10, \pi/2]^\top$, $[0, -10, \pi/2]^\top$, and $[10, -10, \pi/2]^\top$, sequentially. The parameters for (32), (33), and (40)–(42) are specified by $\boldsymbol{Q}_{i1} = \boldsymbol{Q}_{i2} = \boldsymbol{I}_2$, $\boldsymbol{\Lambda}_{iq} = \boldsymbol{\Lambda}_{i\tau} = \boldsymbol{I}_2$, $\boldsymbol{\gamma}_{iq} = 5$, $\boldsymbol{\gamma}_{i\tau} = 4$, $\boldsymbol{\gamma}_{i\omega} = 2$, $\kappa_{i1} = \mathrm{diag}(0.2, 0.5)$, $\kappa_{i2} = \mathrm{diag}(5, 10)$, $\eta_{i1} = 0.5$, $\kappa_{i2} = \mathrm{diag}(1, 1)$, $\eta_{i1} = 0.5$, $\eta_{i2} = 1$, $\eta_{i3} = 10$, and $\Gamma_i = 2$. The simulation test is performed in MATLAB with a runtime of 250 s and a step size of 0.05 s.

The simulation results using the proposed hierarchical optimal formation control method are shown in Figs. 5–9 and Table 2.

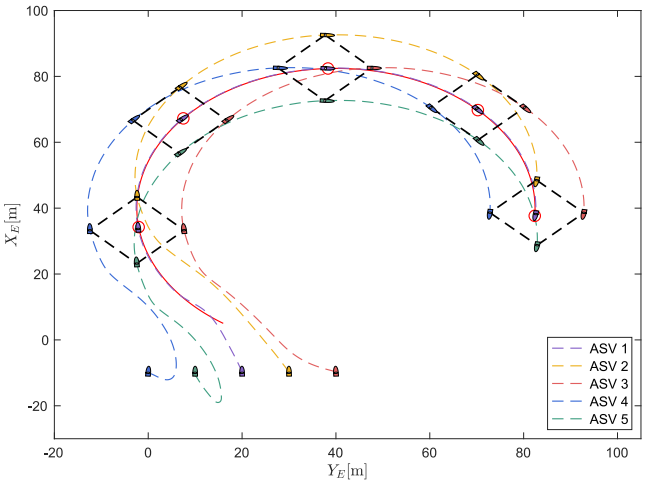

Fig. 5. The motion trajectories of ASVs 1–5 with formation snapshots at 0 s, 50 s, 100 s, 150 s, 200 s, and 250 s.

Table 2
Triggering statistics for coordination and control levels.

Triggering mechanism	ASV No.	Max. interval	Triggering count	Triggering ratio
Coordination Level	1	2.75	156	3.12%
	2	4.05	162	3.24%
	3	4.45	193	3.86%
	4	4.00	278	5.56%
	5	4.10	274	5.48%
Control Level	1	1.85	1475	29.50%
	2	2.05	1476	29.52%
	3	1.55	1490	29.80%
	4	1.70	1515	30.30%
	5	1.40	1476	29.52%

The trajectory of the virtual leader and the actual trajectories of ASVs 1–5 are drawn in Fig. 5. From motion snapshots in Fig. 5, the target tracking formation of ASVs 1–5 is achieved under the intermittent communication. For clarity, Figs. 6–9 display the simulation results during 0–50 s. The sampling velocity errors $e_{iq,s}$ and corresponding triggering thresholds $(d_i + a_{i0})\nabla \hat{V}_{i1}^*/(2\gamma_{iq}^2)$ based on the OEM (15) are presented in Fig. 6. According to Figs. 6 and 7, the next sampling instants $t_{i1,s+1}$ are reset when these thresholds are violated by the sampling errors. It is clear from Fig. 7 that the adjacent sampling intervals $T_{i1,s}$ begin to enlarge as the formation system tends to the stability. The maximum inter-sampling intervals, triggering counts, and triggering ratios of each ASV under the OEM (15) are listed in Table 2. Similar to Fig. 6, Fig. 8 draws the evolution of the control input errors $e_{i\tau,s}$ and triggering thresholds $\nabla \hat{V}_{i2}^*/(2\gamma_{i\tau}^2)$ based on OEM (28). The aperiodic inter-sampling instants for the control level are shown in Fig. 9. And the maximum intervals, triggering counts, and triggering ratios under the OEM (28) are also listed in Table 2.

6. Conclusion

This paper considers an event-triggered formation control problem of underactuated ASVs subject to external disturbances. A hierarchical optimal event-triggered framework is developed by integrating game theory with multi-level event-triggered design. At the coordination level, the optimal guidance velocity and the maximum triggering threshold were obtained via solving the zero-sum differential graphical game, enabling the global Nash equilibrium solutions of all ASVs under the coordination-level

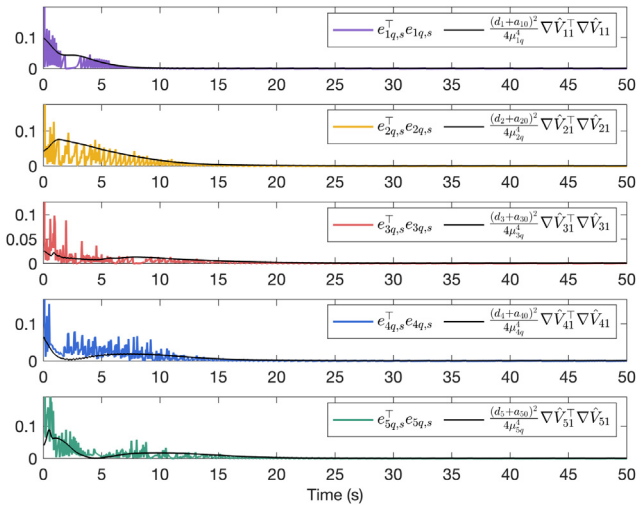

Fig. 6. Sampled velocity errors and triggering thresholds for ASVs 1–5.

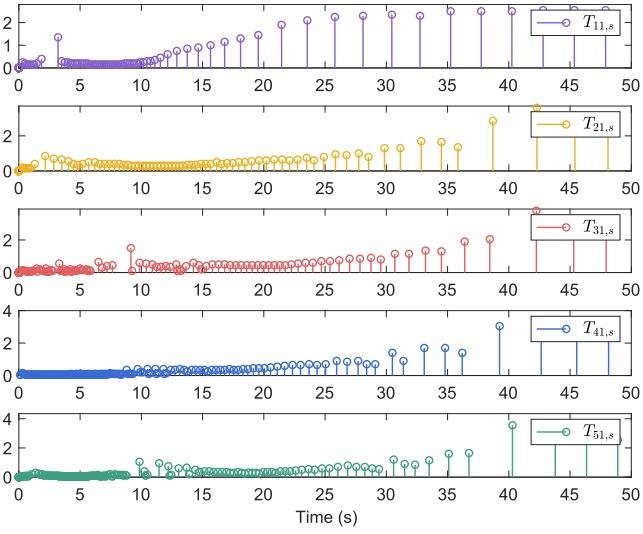

Fig. 7. Aperiodic inter-sample instants for ASVs 1–5.

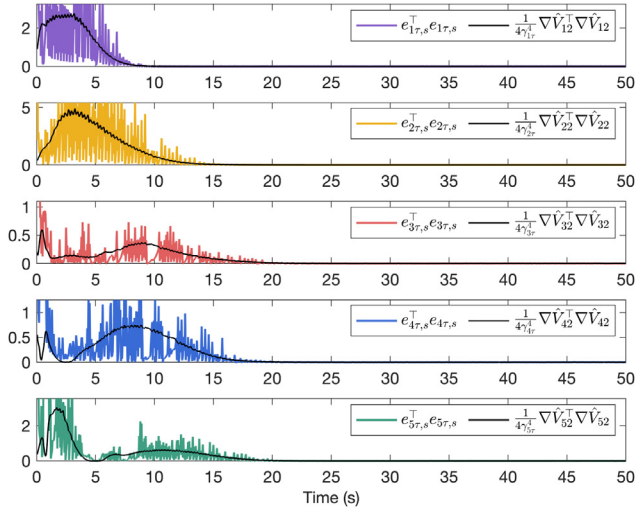

Fig. 8. Sampled control input errors and triggering thresholds for ASVs 1–5.

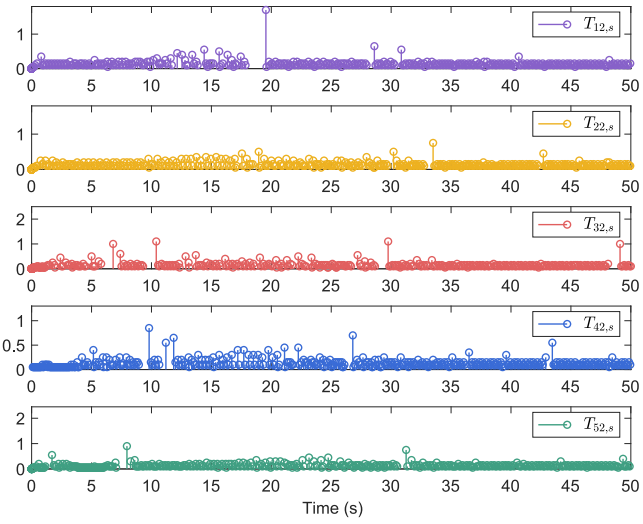

Fig. 9. Aperiodic inter-sample instants for ASVs 1–5.

OEM. Next, a multi-player zero-sum formulation for the control level facilitated the derivation of a robustness-enhanced control policy that accounts for the worst-case disturbances while reducing unnecessary control updates. Then, the online critic-based learning scheme was developed to approximate the associated value functions in real time. Theoretical results show that all signals of closed-loop system are bounded and that Zeno behavior is excluded by ensuring a positive minimum inter-event interval. Finally, simulation results illustrate the effectiveness of the proposed hierarchical framework. Future work will investigate optimal event-triggered formation tracking problems without continuous information broadcasting and monitoring.

Appendix A. Proof of Theorem 1

Define a Lyapunov function candidate $V_{iq} = V_{i1}^*(\boldsymbol{z}_{i1})$ and take its derivative along the dynamics (7) below

$$\begin{aligned}\dot{V}_{iq} =&\nabla V_{i1}^{*\top}\Big((d_i+a_{i0})\boldsymbol{q}_{i,s} - \sum_{j\in\mathcal{N}_i} a_{ij}\boldsymbol{q}_{j,s} - a_{i0}\dot{\boldsymbol{p}}_0\Big)\\ =&\nabla V_{i1}^{*\top}\Big((d_i+a_{i0})(\boldsymbol{q}_i+\boldsymbol{e}_{iq,s})\\ &- \sum_{j\in\mathcal{N}_i} a_{ij}(\boldsymbol{q}_j+\boldsymbol{e}_{jq,s}) - a_{i0}\dot{\boldsymbol{p}}_0\Big).\end{aligned} \tag{45}$$

Then, substituting (12)–(13) into (45) and using $H_{i1}(\boldsymbol{z}_{i1}, \boldsymbol{q}_i^*, \boldsymbol{e}_{iq,s}^*, \nabla V_{i1}^*) = 0$ and $2\gamma_{iq}^2\boldsymbol{e}_{iq,s}^* = (d_i+a_{i0})\nabla V_{i1}^*$ derived from (13), we have

$$\begin{aligned}\dot{V}_{iq} =& -\boldsymbol{z}_{i1}^\top\boldsymbol{Q}_{i1}\boldsymbol{z}_{i1} - \boldsymbol{q}_i^{*\top}\boldsymbol{\Lambda}_{iq}\boldsymbol{q}_i^* + \gamma_{iq}^2\boldsymbol{e}_{iq,s}^{*\top}\boldsymbol{e}_{iq,s}^*\\ &- (d_i+a_{i0})\nabla V_{i1}^{*\top}(\boldsymbol{e}_{iq,s}^* - \boldsymbol{e}_{iq,s})\\ =& -\boldsymbol{z}_{i1}^\top\boldsymbol{Q}_{i1}\boldsymbol{z}_{i1} - \boldsymbol{q}_i^{*\top}\boldsymbol{\Lambda}_{iq}\boldsymbol{q}_i^* + \gamma_{iq}^2\boldsymbol{e}_{iq,s}^{*\top}\boldsymbol{e}_{iq,s}^*\\ &- 2\gamma_{iq}^2\boldsymbol{e}_{iq,s}^{*\top}\boldsymbol{e}_{iq,s}^* + 2\gamma_{iq}^2\boldsymbol{e}_{iq,s}^{*\top}\boldsymbol{e}_{iq,s}.\end{aligned} \tag{46}$$

Note that the fact $\boldsymbol{e}_{iq,s}^\top\boldsymbol{e}_{iq,s} \le \boldsymbol{e}_{iq,s}^{*\top}\boldsymbol{e}_{iq,s}^*$ from (15). Under Assumption 3, then it follows

$$\begin{aligned}\dot{V}_{iq} \le& -\boldsymbol{z}_{i1}^\top\boldsymbol{Q}_{i1}\boldsymbol{z}_{i1} - \frac{(d_i+a_{i0})^2}{4}\nabla V_{i1}^{*\top}\Big(\boldsymbol{\Lambda}_{iq}^{-1} - \frac{\boldsymbol{I}_2}{\gamma_{iq}^2}\Big)\nabla V_{i1}^*\\ \le& -c_{i1}\|\boldsymbol{z}_{i1}\|^2\end{aligned} \tag{47}$$

where $c_{i1} = \lambda_{\min}(\boldsymbol{Q}_{i1}) + \mu_{i1}^2(d_i+a_{i0})^2\lambda_{\min}(\boldsymbol{\Lambda}_{iq}^{-1} - \boldsymbol{I}_2/\gamma_{iq}^2)/4 > 0$ since $\boldsymbol{Q}_{i1} > 0$ and $\boldsymbol{\Lambda}_{iq}^{-1} - \boldsymbol{I}_2/\gamma_{iq}^2 > 0$. Then, one has $\dot{V}_{iq} \le 0$, which

further implies that the event-based system (8) is asymptotically stable, and $V_{i1}^*(\boldsymbol{z}_{i1}(\infty))=0$.

In what follows, we can rewrite J_{i1} as follows

$$\begin{aligned}&J_{i1}(\boldsymbol{z}_{i1},\boldsymbol{q}_i,\boldsymbol{e}_{iq,s})\\&=\int_0^\infty\Big(\pi_{i1}(\boldsymbol{z}_{i1},\boldsymbol{q}_i,\boldsymbol{e}_{iq,s})+\nabla V_{i1}^{*\top}\big((d_i+a_{i0})(\boldsymbol{q}_i+\boldsymbol{e}_{iq,s})\\&\quad-\sum_{j\in\mathcal{N}_i}a_{ij}(\boldsymbol{q}_j+\boldsymbol{e}_{jq,s})-a_{i0}\dot{\boldsymbol{p}}_0\big)\Big)dt+V_{i1}^*(\boldsymbol{z}_{i1}(0)).\end{aligned}$$

From (12) and (13), it results to $-2\boldsymbol{\Lambda}_{iq}\boldsymbol{q}_i^*=(d_i+a_{i0})\nabla V_{i1}^*$ and $2\gamma_{iq}^2\boldsymbol{e}_{iq,s}^*=(d_i+a_{i0})\nabla V_{i1}^*$. Using $H_{i1}(\boldsymbol{z}_{i1},\boldsymbol{q}_i^*,\boldsymbol{e}_{iq,s}^*,\nabla V_{i1}^*)=0$ and assuming the neighbors' policies $\boldsymbol{q}_j=\boldsymbol{q}_j^*$ and $\boldsymbol{e}_{jq,s}=\boldsymbol{e}_{jq,s}^*$, then one has

$$\begin{aligned}&J_{i1}(\boldsymbol{z}_{i1},\boldsymbol{q}_i,\boldsymbol{e}_{iq,s},\boldsymbol{q}_{-i}^*,\boldsymbol{e}_{-iq,s}^*)=V_{i1}^*(\boldsymbol{z}_{i1}(0))\\&+\int_0^\infty(\boldsymbol{q}_i-\boldsymbol{q}_i^*)^\top\boldsymbol{\Lambda}_{iq}(\boldsymbol{q}_i-\boldsymbol{q}_i^*)dt\\&-\int_0^\infty\gamma_{iq}^2(\boldsymbol{e}_{iq,s}-\boldsymbol{e}_{iq,s}^*)^\top(\boldsymbol{e}_{iq,s}-\boldsymbol{e}_{iq,s}^*)dt.\end{aligned}\tag{48}$$

Obviously, it gets from (48) that three cases hold: i) $J_{i1}(\boldsymbol{z}_{i1},\boldsymbol{q}_i^*,\boldsymbol{e}_{iq,s}^*,\boldsymbol{q}_{-i}^*,\boldsymbol{e}_{-iq,s}^*)=V_{i1}^*(\boldsymbol{z}_{i1}(0))$ for $\boldsymbol{q}_i=\boldsymbol{q}_i^*$ and $\boldsymbol{e}_{iq,s}=\boldsymbol{e}_{iq,s}^*$; ii) $J_{i1}(\boldsymbol{z}_{i1},\boldsymbol{q}_i,\boldsymbol{e}_{iq,s}^*,\boldsymbol{q}_{-i}^*,\boldsymbol{e}_{-iq,s}^*)=V_{i1}^*(\boldsymbol{z}_{i1}(0))+\int_0^\infty(\boldsymbol{q}_i-\boldsymbol{q}_i^*)^\top\boldsymbol{\Lambda}_{iq}(\boldsymbol{q}_i-\boldsymbol{q}_i^*)dt$ for $\boldsymbol{q}_i\neq\boldsymbol{q}_i^*$ and $\boldsymbol{e}_{iq,s}=\boldsymbol{e}_{iq,s}^*$; and iii) $J_{i1}(\boldsymbol{z}_{i1},\boldsymbol{q}_i^*,\boldsymbol{e}_{iq,s},\boldsymbol{q}_{-i}^*,\boldsymbol{e}_{-iq,s}^*)=V_{i1}^*(\boldsymbol{z}_{i1}(0))-\int_0^\infty\gamma_{iq}^2(\boldsymbol{e}_{iq,s}-\boldsymbol{e}_{iq,s}^*)^\top(\boldsymbol{e}_{iq,s}-\boldsymbol{e}_{iq,s}^*)dt$ for $\boldsymbol{q}_i=\boldsymbol{q}_i^*$ and $\boldsymbol{e}_{iq,s}\neq\boldsymbol{e}_{iq,s}^*$. Therefore, it yields that the N-tuple policy pair $\{(\boldsymbol{q}_i^*,\boldsymbol{e}_{iq,s}^*)\}_{i=1}^N$ is the global Nash equilibrium and the event-triggered graphical game reaches to the optimal value such that $J_{i1}(\boldsymbol{z}_{i1}(0),\boldsymbol{q}_i^*,\boldsymbol{e}_{iq,s}^*,\boldsymbol{q}_{-i}^*,\boldsymbol{e}_{-iq,s}^*)=V_{i1}^*(\boldsymbol{z}_{i1}(0))$ given by the HJI solution (11). This completes the proof.

Appendix B. proof of Theorem 2

Select a Lyapunov function candidate $V_{i2}^*(\boldsymbol{z}_{i2})$ and follow the similar argument used in the proof of Theorem 1. It concludes that the event-based system (19) is stable under Assumption 2 and $\lim_{t\to\infty}\boldsymbol{z}_{i2}=0$. Further, it gets that the policy pair $(\boldsymbol{\tau}_i^*,\boldsymbol{e}_{i\tau,s}^*,\boldsymbol{\omega}_i^*)$ is the Nash equilibrium of multi-player zero-sum game by $J_{i2}(\boldsymbol{z}_{i2},\boldsymbol{\tau}_i^*,\boldsymbol{e}_{i\tau,s},\boldsymbol{\omega}_i)\le J_{i2}(\boldsymbol{z}_{i2},\boldsymbol{\tau}_i^*,\boldsymbol{e}_{i\tau,s}^*,\boldsymbol{\omega}_i^*)\le J_{i2}(\boldsymbol{z}_{i2},\boldsymbol{\tau}_i,\boldsymbol{e}_{i\tau,s}^*,\boldsymbol{\omega}_i^*)$.

Remark 7. It is observed from (47) that a larger c_{i1} facilitates a faster convergence to the Nash equilibrium for optimization problem (9), which can be achieved by increasing $\boldsymbol{Q}_{i1}$ and γ_{iq}, while decreasing $\boldsymbol{\Lambda}_{iq}$. Similarly, larger values of $\boldsymbol{Q}_{i2}$, $\gamma_{i\tau}$, and $\gamma_{i\omega}$, together with a smaller $\boldsymbol{\Lambda}_{i\tau}$, can accelerate the Nash equilibrium seeking for optimization problem (20). However, such parameter tuning strategies may lead to increased control effort and higher sampling frequency. Therefore, the proper selection of such parameters is desirable to trade off the control performance and computation complexity in practical applications.

Appendix C. proof of Theorem 3

Step 1: Consider a Lyapunov function candidate as

$$L_{i1}=\frac{1}{2}\boldsymbol{z}_{i1}^\top\boldsymbol{z}_{i1}+\frac{1}{2\eta_{ic1}}\tilde{\boldsymbol{\Theta}}_{ic1}^\top\tilde{\boldsymbol{\Theta}}_{ic1}\tag{49}$$

where $\eta_{ic1}>0$ is a constant and $\tilde{\boldsymbol{\Theta}}_{ic1}=\boldsymbol{\Theta}_{ic1}-\hat{\boldsymbol{\Theta}}_{ic1}$.

Then, differentiating (49) along dynamics (8) and (35) as follows

$$\begin{aligned}\dot{L}_{i1}=&\boldsymbol{z}_{i1}^\top\Big((d_i+a_{i0})(\boldsymbol{q}_i+\boldsymbol{e}_{iq,s})-\sum_{j\in\mathcal{N}_i}a_{ij}\boldsymbol{q}_{j,s}-a_{i0}\dot{\boldsymbol{p}}_0\Big)\\&+\frac{\eta_{i1}}{\eta_{ic1}}\tilde{\boldsymbol{\Theta}}_{ic1}^\top\Big(\frac{\boldsymbol{\chi}_{i1}}{b_{i1}^2}e_{ic1}+\sum_{\ell=1}^{N_\ell}\frac{\boldsymbol{\chi}_{i1,\ell}}{b_{i1,\ell}^2}e_{ic1,\ell}\Big).\end{aligned}\tag{50}$$

Substituting (16), (17), (32), and (33), one obtains

$$\begin{aligned}\dot{L}_{i1}=&-\kappa_{i1}\boldsymbol{z}_{i1}^\top\boldsymbol{\zeta}_{i1}^{-1}\boldsymbol{z}_{i1}-\frac{1}{2}\boldsymbol{z}_{i1}^\top\boldsymbol{\zeta}_{i1}^{-1}\boldsymbol{\varphi}_{i1}^\top(\boldsymbol{z}_{i1},\boldsymbol{p}_i)\hat{\boldsymbol{\Theta}}_{ic1}\\&+(d_i+a_{i0})\boldsymbol{z}_{i1}^\top(\boldsymbol{z}_{i2}+\boldsymbol{z}_{iq})-\sum_{j\in\mathcal{N}_i}a_{ij}\boldsymbol{z}_{i1}^\top\boldsymbol{e}_{jq,s}\\&-\frac{\eta_{i1}}{\eta_{ic1}}\tilde{\boldsymbol{\Theta}}_{ic1}^\top\Big(\frac{\boldsymbol{\chi}_{i1}\boldsymbol{\chi}_{i1}^\top}{b_{i1}^2}+\sum_{\ell=1}^{N_\ell}\frac{\boldsymbol{\chi}_{i1,\ell}\boldsymbol{\chi}_{i1,\ell}^\top}{b_{i1,\ell}^2}\Big)\tilde{\boldsymbol{\Theta}}_{ic1}\\&+\frac{\eta_{i1}}{\eta_{ic1}}\frac{\tilde{\boldsymbol{\Theta}}_{ic1}^\top\boldsymbol{\chi}_{i1}}{b_{i1}^2}\check{\boldsymbol{\epsilon}}_{i1}+\frac{\eta_{i1}}{\eta_{ic1}}\sum_{\ell=1}^{N_\ell}\frac{\tilde{\boldsymbol{\Theta}}_{ic1}^\top\boldsymbol{\chi}_{i1,\ell}}{b_{i1,\ell}^2}\check{\boldsymbol{\epsilon}}_{i1,\ell}\end{aligned}\tag{51}$$

with $\check{\boldsymbol{\epsilon}}_{i1}=-\boldsymbol{\epsilon}_{i1}^\top\boldsymbol{\Lambda}_{iq}((d_i+a_{i0})(\hat{\boldsymbol{q}}_i^*+\hat{\boldsymbol{e}}_{iq,s}^*)-\sum_{j\in\mathcal{N}_i}a_{ij}(\boldsymbol{q}_j^*+\boldsymbol{e}_{jq,s}^*)-a_{i0}\dot{\boldsymbol{p}}_0)/(d_i+a_{i0})^2$.

From Young's inequality and $\hat{\boldsymbol{\Theta}}_{ic1}=\boldsymbol{\Theta}_{i1}-\tilde{\boldsymbol{\Theta}}_{ic1}$, it has

$$\begin{aligned}-\boldsymbol{z}_{i1}^\top\boldsymbol{\zeta}_{i1}^{-1}\boldsymbol{\varphi}_{i1}^\top\hat{\boldsymbol{\Theta}}_{ic1}\le&\|\boldsymbol{\zeta}_{i1}^{-1}\|\|\boldsymbol{z}_{i1}\|^2+\frac{1}{2}\|\boldsymbol{\zeta}_{i1}^{-1}\|\|\boldsymbol{\Theta}_{ic1}\|^2\\&+\frac{1}{2}\|\boldsymbol{\zeta}_{i1}^{-1}\|\|\tilde{\boldsymbol{\Theta}}_{ic1}\|^2\end{aligned}\tag{52}$$

$$\frac{\tilde{\boldsymbol{\Theta}}_{ic1}^\top\boldsymbol{\chi}_{i1}}{b_{i1}^2}\check{\boldsymbol{\epsilon}}_{i1}\le\frac{\tilde{\boldsymbol{\Theta}}_{ic1}^\top\boldsymbol{\chi}_{i1}\boldsymbol{\chi}_{i1}^\top\tilde{\boldsymbol{\Theta}}_{ic1}}{2b_{i1}^2}+\frac{\|\check{\boldsymbol{\epsilon}}_{i1}\|^2}{2}\tag{53}$$

$$\frac{\tilde{\boldsymbol{\Theta}}_{ic1}^\top\boldsymbol{\chi}_{i1,\ell}}{b_{i1,\ell}^2}\check{\boldsymbol{\epsilon}}_{i1,\ell}\le\frac{\tilde{\boldsymbol{\Theta}}_{ic1}^\top\boldsymbol{\chi}_{i1,\ell}\boldsymbol{\chi}_{i1,\ell}^\top\tilde{\boldsymbol{\Theta}}_{ic1}}{2b_{i1,\ell}^2}+\frac{\|\check{\boldsymbol{\epsilon}}_{i1,\ell}\|^2}{2}.\tag{54}$$

Thus, synthesizing (51)–(54) yields

$$\begin{aligned}\dot{L}_{i1}\le&-\Big(\frac{\kappa_{i1}}{\lambda_{\max}(\boldsymbol{\zeta}_{i1})}-\frac{1}{2}\|\boldsymbol{\zeta}_{i1}^{-1}\|-\frac{3}{2}d_i-a_{i0}\Big)\|\boldsymbol{z}_{i1}\|^2\\&-\Big(\frac{\eta_{i1}}{2\eta_{ic1}}\underline{\lambda}_{i\chi1}-\frac{1}{4}\|\boldsymbol{\zeta}_{i1}^{-1}\|\Big)\|\tilde{\boldsymbol{\Theta}}_{ic1}\|^2\\&+\frac{1}{2}(d_i+a_{i0})\big(\|\boldsymbol{z}_{i2}\|^2+\|\boldsymbol{z}_{iq}\|^2\big)+\varrho_{i1}\end{aligned}\tag{55}$$

with $\underline{\lambda}_{i\chi1}=\lambda_{\min}(\boldsymbol{\chi}_{i1}\boldsymbol{\chi}_{i1}^\top/b_{i1}^2+\sum_{\ell=1}^{N_\ell}\boldsymbol{\chi}_{i1,\ell}\boldsymbol{\chi}_{i1,\ell}^\top/b_{i1,\ell}^2)$, and $\varrho_{i1}=\bar{\theta}_{i1}^2\|\boldsymbol{\zeta}_{i1}^{-1}\|/4+\bar{o}_{iq}/2+(N_\ell+1)\eta_{i1}\bar{\epsilon}_{i1}^2/2\eta_{ic1}$ under Assumptions 1–2, where $\bar{o}_{iq}>0$ and $\bar{\epsilon}_{i1}>0$ present upper bound of $\sum_{j\in\mathcal{N}_i}a_{ij}\|\boldsymbol{e}_{jq,s}\|^2$ and $\|\check{\boldsymbol{\epsilon}}_{i1}\|$ from Wu, Chen, Li, and Chadli (2024), respectively.

Step 2: Construct a Lyapunov function candidate

$$L_{i2}=\frac{\boldsymbol{z}_{i2}^\top\boldsymbol{z}_{i2}}{2}+\frac{\boldsymbol{z}_{iq}^\top\boldsymbol{z}_{iq}}{2}+\frac{\tilde{\boldsymbol{\Theta}}_{ic2}^\top\tilde{\boldsymbol{\Theta}}_{ic2}}{2\eta_{ic2}}+\frac{\tilde{\boldsymbol{\Theta}}_{i\sigma}^\top\tilde{\boldsymbol{\Theta}}_{i\sigma}}{2\Gamma_i}\tag{56}$$

where $\eta_{ic2}>0$ is a constant, and $\tilde{\boldsymbol{\Theta}}_{ic2}=\boldsymbol{\Theta}_{ic2}-\hat{\boldsymbol{\Theta}}_{ic2}$ and $\tilde{\boldsymbol{\Theta}}_{i\sigma}=\boldsymbol{\Theta}_{i\sigma}-\hat{\boldsymbol{\Theta}}_{i\sigma}$ denote the estimation errors.

Based on (19), (37), (43) and (44), the time derivative of L_{i2} is taken as

$$\begin{aligned}\dot{L}_{i2}=&\boldsymbol{z}_{i2}^\top\Big(\boldsymbol{\varphi}_{i\sigma}^\top\boldsymbol{\Theta}_{i\sigma}+\boldsymbol{\epsilon}_{i\sigma}+\boldsymbol{\tau}_i+\boldsymbol{e}_{i\tau,s}+\boldsymbol{\omega}_i+\frac{\boldsymbol{z}_{iq}}{\kappa_{i\alpha}}\Big)\\&-\boldsymbol{z}_{iq}^\top\Big(\frac{\boldsymbol{z}_{iq}}{\kappa_{i\alpha}}+\dot{\hat{\boldsymbol{q}}}_i^*\Big)-\tilde{\boldsymbol{\Theta}}_{i\sigma}^\top(\boldsymbol{\varphi}_{i\sigma}\boldsymbol{z}_{i2}-\eta_{i3}\hat{\boldsymbol{\Theta}}_{i\sigma})\\&+\frac{\eta_{i2}}{\eta_{ic2}}\tilde{\boldsymbol{\Theta}}_{ic2}^\top\Big(\frac{\boldsymbol{\chi}_{i2}}{b_{i2}^2}e_{ic2}-\sum_{\ell=1}^{N_\ell}\frac{\boldsymbol{\chi}_{i2,\ell}}{b_{i2,\ell}^2}e_{ic2,\ell}\Big).\end{aligned}\tag{57}$$

Substituting (40)–(42) into (57), we have

$$\dot{L}_{i2}=\boldsymbol{z}_{i2}^\top\Big(\boldsymbol{\varphi}_{i\sigma}^\top\boldsymbol{\Theta}_{i\sigma}+\boldsymbol{\epsilon}_{i\sigma}+\frac{\boldsymbol{z}_{iq}}{\kappa_{i\alpha}}\Big)$$

$$+ \boldsymbol{z}_{i2}^{\top}\left(\frac{\boldsymbol{\Lambda}_{i\tau}}{\gamma_{i\tau}^2}+\frac{\boldsymbol{\Lambda}_{i\tau}}{\gamma_{i\omega}^2}-\boldsymbol{I}_2\right)\Big(\kappa_{i2}\boldsymbol{z}_{i2}+\boldsymbol{\zeta}_{i2}\boldsymbol{\varphi}_{i\sigma}^{\top}\hat{\boldsymbol{\Theta}}_{i\sigma} + \frac{1}{\kappa_{i\alpha}}\boldsymbol{\zeta}_{i2}\boldsymbol{z}_{iq}+\frac{1}{2}\boldsymbol{\varphi}_{i2}^{\top}(\boldsymbol{z}_{i2},\boldsymbol{q}_i)\hat{\boldsymbol{\Theta}}_{ic2}\Big) - \boldsymbol{z}_{iq}^{\top}\left(\frac{\boldsymbol{z}_{iq}}{\kappa_{i\alpha}}+\dot{\hat{\boldsymbol{q}}}_i^{*}\right) - \tilde{\boldsymbol{\Theta}}_{i\sigma}^{\top}(\boldsymbol{\varphi}_{i\sigma}\boldsymbol{z}_{i2}-\eta_{i3}\hat{\boldsymbol{\Theta}}_{i\sigma}) - \frac{\eta_{i2}}{\eta_{ic2}}\tilde{\boldsymbol{\Theta}}_{ic2}^{\top}\left(\frac{\boldsymbol{\chi}_{i2}\boldsymbol{\chi}_{i2}^{\top}}{b_{i2}^2}+\sum_{\ell=1}^{N_\ell}\frac{\boldsymbol{\chi}_{i2,\ell}\boldsymbol{\chi}_{i2,\ell}^{\top}}{b_{i2,\ell}^2}\right)\tilde{\boldsymbol{\Theta}}_{ic2} + \frac{\eta_{i2}}{\eta_{ic2}}\left(\frac{\tilde{\boldsymbol{\Theta}}_{ic2}^{\top}\boldsymbol{\chi}_{i2}}{b_{i2}^2}\breve{\boldsymbol{\epsilon}}_{i2}+\sum_{\ell=1}^{N_\ell}\frac{\tilde{\boldsymbol{\Theta}}_{ic2}^{\top}\boldsymbol{\chi}_{i2,\ell}}{b_{i2,\ell}^2}\breve{\boldsymbol{\epsilon}}_{i2,\ell}\right) \tag{58}$$

where $\breve{\boldsymbol{\epsilon}}_{i2}=-\boldsymbol{\epsilon}_{i2}^{\top}\boldsymbol{\Lambda}_{i\tau}(\hat{\boldsymbol{\Theta}}_{i\sigma}^{\top}\boldsymbol{\varphi}_{i\sigma}(\boldsymbol{q}_i)+\hat{\boldsymbol{\tau}}_i^{*}+\hat{\boldsymbol{e}}_{i\tau,s}^{*}+\hat{\boldsymbol{\omega}}_i^{*}+\boldsymbol{z}_{iq}/\kappa_{i\alpha})$.

According to Young's inequality and $\tilde{\boldsymbol{\Theta}}_{ic2}=\boldsymbol{\Theta}_{ic2}-\hat{\boldsymbol{\Theta}}_{ic2}$, we have

$$-\boldsymbol{z}_{i2}^{\top}\boldsymbol{\zeta}_{i2}^{-1}\boldsymbol{\varphi}_{i2}^{\top}\hat{\boldsymbol{\Theta}}_{ic2}\le\|\boldsymbol{\zeta}_{i2}^{-1}\|\|\boldsymbol{z}_{i2}\|^2+\frac{1}{2}\|\boldsymbol{\zeta}_{i2}^{-1}\|\|\boldsymbol{\Theta}_{ic2}\|^2+\frac{1}{2}\|\boldsymbol{\zeta}_{i2}^{-1}\|\|\tilde{\boldsymbol{\Theta}}_{ic2}\|^2 \tag{59}$$

$$\frac{\tilde{\boldsymbol{\Theta}}_{ic2}^{\top}\boldsymbol{\chi}_{i2}}{b_{i2}^2}\breve{\boldsymbol{\epsilon}}_{i2}\le\frac{\tilde{\boldsymbol{\Theta}}_{ic2}^{\top}\boldsymbol{\chi}_{i2}\boldsymbol{\chi}_{i2}^{\top}\tilde{\boldsymbol{\Theta}}_{ic2}}{2b_{i2,\ell}^2}+\frac{\|\breve{\boldsymbol{\epsilon}}_{i2}\|^2}{2} \tag{60}$$

$$\frac{\tilde{\boldsymbol{\Theta}}_{ic2}^{\top}\boldsymbol{\chi}_{i2,\ell}}{b_{i2,\ell}^2}\breve{\boldsymbol{\epsilon}}_{i2,\ell}\le\frac{\tilde{\boldsymbol{\Theta}}_{ic2}^{\top}\boldsymbol{\chi}_{i2,\ell}\boldsymbol{\chi}_{i2,\ell}^{\top}\tilde{\boldsymbol{\Theta}}_{ic2}}{2b_{i2,\ell}^2}+\frac{\|\breve{\boldsymbol{\epsilon}}_{i2,\ell}\|^2}{2}. \tag{61}$$

Then, taking inequalities (59)–(61) into (58) yields

$$\dot{L}_{i2}\le-\left(\frac{\kappa_{i2}}{\lambda_{\max}(\boldsymbol{\zeta}_{i2})}-\frac{1}{2}\|\boldsymbol{\zeta}_{i2}^{-1}\|-\frac{1}{2}\right)\|\boldsymbol{z}_{i2}\|^2-\left(\frac{1}{\kappa_{i\alpha}}-\frac{1}{2}\right)\|\boldsymbol{z}_{iq}\|^2-\frac{\eta_{i3}}{2}\|\tilde{\boldsymbol{\Theta}}_{i\sigma}\|^2-\left(\frac{\eta_{i2}}{2\eta_{ic2}}\underline{\lambda}_{i2,\chi}-\frac{1}{4}\|\boldsymbol{\zeta}_{i2}^{-1}\|\right)\|\tilde{\boldsymbol{\Theta}}_{ic2}\|^2+\varrho_{i2} \tag{62}$$

with $\underline{\lambda}_{i2,\chi}=\lambda_{\min}(\sum_{\ell=1}^{N_\ell}\boldsymbol{\chi}_{i2,\ell}\boldsymbol{\chi}_{i2,\ell}^{\top}/b_{i2,\ell}^2+\boldsymbol{\chi}_{i2}\boldsymbol{\chi}_{i2}^{\top}/b_{i2}^2)$ and $\varrho_{i2}=\bar{\epsilon}_{i\sigma}^2/2+\bar{o}_{i\tau1}/2+\eta_{i3}\bar{\theta}_{i\sigma}^2/2+\bar{\theta}_{ic2}^2\|\boldsymbol{\zeta}_{i2}^{-1}\|/4+(N_\ell+1)\bar{\epsilon}_{i2}^2\|\boldsymbol{\Lambda}_{i\tau}\|^2\bar{o}_{i\tau2}^2\eta_{i2}/2\eta_{ic2}$, where $\bar{o}_{i\tau1}>0$ is the upper bound of $\|\dot{\hat{\boldsymbol{q}}}_i^{*}\|^2$, and $\bar{o}_{i\tau2}>0$ stands for the maximum value of $o_{i\tau2}=\hat{\boldsymbol{\Theta}}_{i\sigma}^{\top}\boldsymbol{\varphi}_{i\sigma}(\boldsymbol{q}_i)+\hat{\boldsymbol{\tau}}_i^{*}+\hat{\boldsymbol{e}}_{i\tau,s}^{*}+\hat{\boldsymbol{\omega}}_i^{*}+\boldsymbol{z}_{iq}/\kappa_{i\alpha}$.

To elaborate the stability of the closed-loop system, consider a total Lyapunov function $L_i=L_{i1}+L_{i2}$. Based on the above results (55) and (62), it has the time derivative of L_i as follows

$$\dot{L}_i\le-\tilde{\kappa}_{i1}\|\boldsymbol{z}_{i1}\|^2-\tilde{\kappa}_{i2}\|\boldsymbol{z}_{i2}\|^2-\tilde{\kappa}_{i\alpha}\|\boldsymbol{z}_{iq}\|^2-\tilde{\eta}_{i1}\|\tilde{\boldsymbol{\Theta}}_{ic1}\|^2-\tilde{\eta}_{i2}\|\tilde{\boldsymbol{\Theta}}_{ic2}\|^2-\tilde{\eta}_{i3}\|\tilde{\boldsymbol{\Theta}}_{i\sigma}\|^2+\varrho_i \tag{63}$$

where $\tilde{\kappa}_{i1}=\kappa_{i1}/\lambda_{\max}(\boldsymbol{\zeta}_{i1})-\|\boldsymbol{\zeta}_{i1}^{-1}\|/2-3d_i/2-a_{i0}$, $\tilde{\kappa}_{i2}=\kappa_{i2}/\lambda_{\max}(\boldsymbol{\zeta}_{i2})-(d_i+a_{i0}+1)/2-\|\boldsymbol{\zeta}_{i2}^{-1}\|/2$, $\tilde{\kappa}_{i\alpha}=1/\kappa_{i\alpha}-(d_i+a_{i0}+1)/2$, $\tilde{\eta}_{i1}=\eta_{i1}\underline{\lambda}_{i\chi1}/2\eta_{ic1}-\|\boldsymbol{\zeta}_{i1}^{-1}\|/4$, $\tilde{\eta}_{i2}=\eta_{i2}\underline{\lambda}_{i2,\chi}/2\eta_{ic2}-\|\boldsymbol{\zeta}_{i2}^{-1}\|/4$, $\tilde{\eta}_{i3}=3\eta_{i3}/2$, and $\varrho_i=\varrho_{i1}+\varrho_{i2}$.

Then, it yields from (63) that the total Lyapunov function $L=\sum_{i=1}^{N}L_i$ satisfies

$$\dot{L}\le-\rho L+\varrho \tag{64}$$

where $\rho=\min_{i\in\mathbb{I}}\rho_i$ and $\varrho=\sum_{i=1}^{N}\varrho_i$ with $\rho_i=\min\{2\tilde{\kappa}_{i1},2\tilde{\kappa}_{i2},\tilde{\kappa}_{i\alpha},2\eta_{ic1}\tilde{\eta}_{i1},2\eta_{ic2}\tilde{\eta}_{i2},2\Gamma_i\tilde{\eta}_{i3}\}$. It can see that $\dot{L}<0$ by selecting suitable parameters such that $\tilde{\kappa}_{i1}>0$, $\tilde{\kappa}_{i2}>0$, $\tilde{\kappa}_{i\alpha}>0$, $\tilde{\eta}_{i1}>0$, $\tilde{\eta}_{i2}>0$, and $\tilde{\eta}_{i3}>0$, as well as $\boldsymbol{E}_i=[\boldsymbol{z}_{i1}^{\top},\boldsymbol{z}_{i2}^{\top},\boldsymbol{z}_{iq}^{\top},\tilde{\boldsymbol{\Theta}}_{ic1}^{\top},\tilde{\boldsymbol{\Theta}}_{ic2}^{\top},\tilde{\boldsymbol{\Theta}}_{i\sigma}^{\top}]^{\top}$ locates outside the compact set given by

$$\Omega_{iE}=\left\{\boldsymbol{E}_i\mid\|\boldsymbol{E}_i\|\le\sqrt{\frac{\varrho}{\rho_i}}\right\}.$$

Therefore, the closed-loop system is guaranteed to be UUB using the proposed optimal event-triggered formation control framework.

In the subsequent part, let us prove that the Zeno behavior can be excluded. For the coordination level, define $\boldsymbol{e}_{iz1}=\boldsymbol{z}_{i1,s}-\boldsymbol{z}_{i1}$ and take its time derivative with (8), (32), and (33) as follows

$$\dot{\boldsymbol{e}}_{iz1}=\kappa_{i1}\boldsymbol{\zeta}_{i1}^{-1}\boldsymbol{z}_{i1}-(d_i+a_{i0})(\boldsymbol{z}_{i2}+\boldsymbol{z}_{iq})+\frac{1}{2}\boldsymbol{\zeta}_{i1}^{-1}\boldsymbol{\varphi}_{i1}^{\top}(\boldsymbol{z}_{i1},\boldsymbol{p}_i)\hat{\boldsymbol{\Theta}}_{ic1}+\sum_{j\in\mathcal{N}_i}a_{ij}\boldsymbol{e}_{jq,s}. \tag{65}$$

According to the above analysis, one knows that $\boldsymbol{z}_{i2}$, $\boldsymbol{z}_{iq}$, and $\hat{\boldsymbol{\Theta}}_{ic1}$ are subsequently bounded by $\bar{z}_{i2}$, $\bar{z}_{iq}$, and $\bar{\hat{\theta}}_{ic1}$ with $\bar{z}_{i2}>0$, $\bar{z}_{iq}>0$, and $\bar{\hat{\theta}}_{ic1}>0$. In addition, the term $\sum_{j\in\mathcal{N}_i}a_{ij}\boldsymbol{e}_{jq,s}$ is also bounded by $\|\sum_{j\in\mathcal{N}_i}a_{ij}\boldsymbol{e}_{jq,s}\|\le\bar{\varpi}_{ij}$ with $\bar{\varpi}_{ij}>0$. Hence, for $t\in[t_{i1,s},t_{i1,s+1})$, one has

$$\|\dot{\boldsymbol{e}}_{iz1}\|\le\frac{\kappa_{i1}}{\lambda_{\min}(\boldsymbol{\zeta}_{i1})}(\|\boldsymbol{e}_{iz1}\|+\|\boldsymbol{z}_{i1,s}\|)+\bar{\hbar}_{i1} \tag{66}$$

with $\bar{\hbar}_{i1}=\bar{\hat{\theta}}_{ic1}/2\lambda_{\min}(\boldsymbol{\zeta}_{i1})+(d_i+a_{i0})(\bar{z}_{i2}+\bar{z}_{iq})/2+\bar{\varpi}_{ij}$. Then, integrating (66) obtains

$$\|\boldsymbol{e}_{iz1}(t)\|\le\left(\|\boldsymbol{z}_{i1,s}\|+\frac{\bar{\hbar}_{i1}\lambda_{\min}(\boldsymbol{\zeta}_{i1})}{\kappa_{i1}}\right)\left(e^{\frac{\kappa_{i1}(t-t_{i1,s})}{\lambda_{\min}(\boldsymbol{\zeta}_{i1})}}-1\right)$$

which yields that

$$T_{i1,s}\ge\frac{\lambda_{\min}(\boldsymbol{\zeta}_{i1})}{\kappa_{i1}}\ln(\Psi_{i1}+1)>0 \tag{67}$$

with $\Psi_{i1}=\kappa_{i1}\|\boldsymbol{e}_{iz1}(t_{i1,s+1})\|/(\kappa_{i1}\|\boldsymbol{z}_{i1,s}\|+\bar{\hbar}_{i1}\lambda_{\min}(\boldsymbol{\zeta}_{i1}))$. It further follows that the minimum sampling interval is $T_{i1,\min}=\lambda_{\min}(\boldsymbol{\zeta}_{i1})\ln(\Psi_{i1,\min}+1)/\kappa_{i1}$ using the minimum value $\Psi_{i1,\min}$ of Ψ_{i1}. It is obvious that $T_{i1,\min}>0$, implying the Zeno-free behavior.

Repeating the above treatment, it gets that the sampling interval $T_{i2,s}$ for the control level holds

$$T_{i2,s}\ge\frac{\lambda_{\min}(\boldsymbol{\zeta}_{i2})}{\kappa_{i2}}\ln(\Psi_{i2,\min}+1)>0$$

with $\Psi_{i2}=\kappa_{i2}\|\boldsymbol{e}_{iz2}(t_{i2,s+1})\|/(\kappa_{i2}\|\boldsymbol{z}_{i2,s}\|+\lambda_{\min}(\boldsymbol{\zeta}_{i2})\bar{\hbar}_{i2})$ and its minimum value $\Psi_{i2,\min}=\min_{s\in\mathbb{N}}\Psi_{i2}$, where $\boldsymbol{e}_{iz2}(t_{i2,s+1})=\boldsymbol{z}_{i2,s}-\boldsymbol{z}_{i2}(t_{i2,s+1})$, $\bar{\hbar}_{i1}=\bar{\hat{\theta}}_{i\sigma}+\bar{\hat{\theta}}_{ic2}+\bar{\epsilon}_{i\sigma}$, and $\bar{\hat{\theta}}_{ic2}>0$ and $\bar{\tilde{\theta}}_{i\sigma}>0$ denote upper bounds of $\hat{\Theta}_{ic2}$ and $\tilde{\Theta}_{i\sigma}$, respectively. Hence, it ensures no Zeno behavior in the control level.

Synthesizing the analysis for both coordination and control levels, it is concluded that the closed-loop system can be guaranteed to exhibit Zeno-free behaviors. This completes the proof.

References

Balch, T., & Arkin, R. C. (1998). 'Behavior-based formation control for multirobot teams. *IEEE Transactions on Robotics and Automation*, *14*(6), 926–939.

Beard, R., Lawton, J., & Hadaegh, F. (2001). A coordination architecture for spacecraft formation control. *IEEE Transactions on Control Systems Technology*, *9*(6), 777–790.

Breivik, M., & Fossen, T. I. (2008). Guidance laws for planar motion control. In *2008 47th IEEE conference on decision and control* (pp. 570–577).

Breivik, M., Hovstein, V. E., & Fossen, T. I. (2008). Straight-line target tracking for unmanned surface vehicles. *Modeling, Identification and Control*, *29*(4), 131–149.

Chowdhary, G., & Johnson, E. (2010). Concurrent learning for convergence in adaptive control without persistency of excitation. In *49th IEEE conference on decision and control* (pp. 3674–3679).

Dai, S.-L., He, S., Lin, H., & Wang, C. (2018). Platoon formation control with prescribed performance guarantees for USVs. *IEEE Transactions on Industrial Electronics*, *65*(5), 4237–4246.

Dai, S., Wu, Z., Zhang, P., Tan, M., & Yu, J. (2023). Distributed formation control for a multirobotic fish system with model-based event-triggered communication mechanism. *IEEE Transactions on Industrial Electronics*, *70*(11), 11433–11442.

Ding, L., Han, Q., Ge, X., & Zhang, X. (2018). An overview of recent advances in event-triggered consensus of multiagent systems. *IEEE Transactions on Cybernetics*, *48*(4), 1110–1123.

Fossen, T. I. (2011). *Handbook of marine craft hydrodynamics and motion control*. John Wiley & Sons.

Gao, J., Proctor, A. A., Shi, Y., & Bradley, C. (2015). Hierarchical model predictive image-based visual servoing of underwater vehicles with adaptive neural network dynamic control. *IEEE Transactions on Cybernetics*, *46*(10), 2323–2334.

Gommans, T., Antunes, D., Donkers, T., Tabuada, P., & Heemels, M. (2014). Self-triggered linear quadratic control. *Automatica*, *50*(4), 1279–1287.

Gu, N., Wang, D., Peng, Z., & Liu, L. (2019). Observer-based finite-time control for distributed path maneuvering of underactuated unmanned surface vehicles with collision avoidance and connectivity preservation. *IEEE Transactions on Systems, Man, and Cybernetics: Systems*, *51*(8), 5105–5115.

Gu, N., Wang, D., Peng, Z., Wang, J., & Han, Q.-L. (2022). Disturbance observers and extended state observers for marine vehicles: A survey. *Control Engineering Practice*, *123*, Article 105158.

Huang, B., Peng, H., Zhang, C., & Ahn, C. K. (2024). Distributed optimal coordinated control for unmanned surface vehicles with interleaved periodic event-based mechanism. *IEEE Transactions on Vehicular Technology*, *73*(12), 18073–18086.

Ihle, I.-A. F., Jouffroy, J., & Fossen, T. I. (2006). Formation control of marine surface craft: A Lagrangian approach. *IEEE Journal of Oceanic Engineering*, *31*(4), 922–934.

Jin, X. (2016). Fault tolerant finite-time leader–follower formation control for autonomous surface vessels with los range and angle constraints. *Automatica*, *68*, 228–236.

Khalil, H. K. (2002). *Nonlinear systems* (3rd ed.) (p. 115). Patience Hall.

Liang, C.-D., Ge, M.-F., Liu, Z.-W., & Ling, F. (2021). Predefined-time formation tracking control of networked marine surface vehicles. *Control Engineering Practice*, *107*, Article 104682.

Lu, K., Dai, S.-L., & Jin, X. (2024). Cooperative constrained enclosing control of multirobot systems in obstacle environments. *IEEE Transactions on Control of Network Systems*, *11*(2), 718–730.

Lu, Y., Su, R., Zhang, C., & Qiao, L. (2022). Event-triggered adaptive formation keeping and interception scheme for autonomous surface vehicles under malicious attacks. *IEEE Transactions on Industrial Informatics*, *18*(6), 3947–3957.

Mazo, M., & Tabada, P. (2008). On event-triggered and self-triggered control over sensor/actuator networks. In *2008 47th IEEE conference on decision and control* (pp. 435–440). IEEE.

Paliotta, C., Lefeber, E., Pettersen, K. Y., Pinto, J., Costa, M., et al. (2018). Trajectory tracking and path following for underactuated marine vehicles. *IEEE Transactions on Control Systems Technology*, *27*(4), 1423–1437.

Pan, J., Han, T., Xiao, B., & Yan, H. (2024). Predefined-time bipartite time-varying formation tracking control of networked autonomous surface vehicles via hierarchical control approach. *Transactions on Vehicular Technology*, *73*(7), 9536–9545.

Park, B. S., & Yoo, S. J. (2021). Connectivity-maintaining and collision-avoiding performance function approach for robust leader–follower formation control of multiple uncertain underactuated surface vessels. *Automatica*, *127*, Article 109501.

Peng, Z., Jiang, Y., & Wang, J. (2021). Event-triggered dynamic surface control of an underactuated autonomous surface vehicle for target enclosing. *IEEE Transactions on Industrial Electronics*, *68*(4), 3402–3412.

Peng, Z., Wang, D., Chen, Z., Hu, X., & Lan, W. (2013). Adaptive dynamic surface control for formations of autonomous surface vehicles with uncertain dynamics. *IEEE Transactions on Control Systems Technology*, *21*(2), 513–520.

Peng, Z., Wang, J., Wang, D., & Han, Q.-L. (2021). An overview of recent advances in coordinated control of multiple autonomous surface vehicles. *IEEE Transactions on Industrial Informatics*, *17*(2), 732–745.

Reis, J., Yu, G., & Silvestre, C. (2023). Kalman-based velocity-free trajectory tracking control of an underactuated aerial vehicle with unknown system dynamics. *Automatica*, *155*, Article 111148.

Ren, W., & Beard, R. W. (2008). *Distributed consensus in multi-vehicle cooperative control*: *Vol. 27*, Springer.

Ringbäck, R., Wei, J., Erstorp, E. S., Kuttenkeuler, J., Johansen, T. A., & Johansson, K. H. (2020). Multi-agent formation tracking for autonomous surface vehicles. *IEEE Transactions on Control Systems Technology*, *29*(6), 2287–2298.

Sahoo, A., Narayanan, V., & Jagannathan, S. (2018). A min–max approach to event-and self-triggered sampling and regulation of linear systems. *IEEE Transactions on Industrial Electronics*, *66*(7), 5433–5440.

Shi, Y., Hu, Q., Li, D., & Lv, M. (2023). Adaptive optimal tracking control for spacecraft formation flying with event-triggered input. *IEEE Transactions on Industrial Informatics*, *19*(5), 6418–6428.

Shi, Y., Shen, C., Fang, H., & Li, H. (2017). Advanced control in marine mechatronic systems: A survey. *IEEE/ASME Transactions on Mechatronics*, *22*(3), 1121–1131.

Shojaei, K. (2015). Leader–follower formation control of underactuated autonomous marine surface vehicles with limited torque. *Ocean Engineering*, *105*, 196–205.

Tang, C., Zhang, H.-T., & Wang, J. (2023). Flexible formation tracking control of multiple unmanned surface vessels for navigating through narrow channels with unknown curvatures. *IEEE Transactions on Industrial Electronics*, *70*(3), 2927–2938.

Wang, W., Li, Y., & Tong, S. (2025). Exact-optimal consensus of uncertain nonlinear multi-agent systems based on fuzzy approximation. *IEEE Transactions on Automation Science and Engineering*, *22*, 1497–1507.

Wang, P., Liang, X., Peng, X., Lu, Y., & Ge, S. S. (2024). Control barrier performance function-based cooperative formation with parallel dynamic event-triggering strategy. *IEEE Transactions on Systems, Man, and Cybernetics: Systems*, *54*(7), 4552–4564.

Wu, Y., Chen, M., Chadli, M., & Li, H. (2024). Dual-type-triggers-based cooperative adaptive critic control of swarm UAVs under FDI attacks. *Automatica*, *167*, Article 111757.

Wu, Y., Chen, M., Li, H., & Chadli, M. (2024). Mixed-zero-sum-game-based memory event-triggered cooperative control of heterogeneous MASs against DoS attacks. *IEEE Transactions on Cybernetics*, *54*(10), 5733–5745.

Wu, W., Peng, Z., Liu, L., & Wang, D. (2022). A general safety-certified cooperative control architecture for interconnected intelligent surface vehicles with applications to vessel train. *IEEE Transactions on Intelligent Vehicles*, *7*(3), 627–637.

Wu, W., Peng, Z., Wang, D., Liu, L., & Han, Q.-L. (2022). Network-based line-of-sight path tracking of underactuated unmanned surface vehicles with experiment results. *IEEE Transactions on Cybernetics*, *52*(10), 10937–10947.

Wu, W., Zhang, Y., Jia, Z., Lu, J.-G., & Zhang, W. (2024). Adaptive fault-tolerant fuzzy containment control for networked autonomous surface vehicles: A noncooperative game approach. *IEEE Transactions on Fuzzy Systems*, *32*(7), 4192–4204.

Wu, W., Zhang, Y., Li, Z., Lu, J.-G., & Zhang, W. (2024). Constrained safe cooperative maneuvering of autonomous surface vehicles: A control barrier function approach. *IEEE Transactions on Systems, Man, and Cybernetics: Systems*, 1–12.

Xu, W., Wang, T., Qiu, J., & Liu, X. (2024). A novel framework for game-based optimal event-triggered control of multi-input nonlinear systems. *IEEE Transactions on Automatic Control*, *69*(7), 4867–4874.

Xu, B., Zhang, H.-T., Ding, Y., & Ren, W. (2023). Event-triggered surrounding formation control of multiagent systems for multiple dynamic targets. *IEEE Transactions on Control of Network Systems*, *10*(2), 752–764.

Ye, M., Ding, L., Han, Q.-L., Shi, J., & Shen, C. (2025). Distributed optimal formation tracking of multiple noncooperative targets: A time-varying game-based approach. *Automatica*, *173*, Article 112074.

Yu, K., Li, Y., Lv, M., & Tong, S. (2024). Distributed optimal formation control of multiple unmanned surface vehicles with stackelberg differential graphical game. *IEEE Transactions on artificial intelligence*, *5*(8), 4058–4073.

Zhang, L., Che, W.-W., Deng, C., & Wu, Z.-G. (2022). Prescribed performance control for multiagent systems via fuzzy adaptive event-triggered strategy. *IEEE Transactions on Fuzzy Systems*, *30*(12), 5078–5090.

Zhang, Y., Wu, W., & Zhang, W. (2023). Noncooperative game-based cooperative maneuvering of intelligent surface vehicles via accelerated learning-based neural predictors. *IEEE Transactions on Intelligent Vehicles*, *8*(3), 2212–2221.

Zhao, M., & Li, H. (2024). Distributed model predictive contouring control of unmanned surface vessels. *IEEE Transactions on Industrial Electronics*, *71*(10), 13012–13019.

Zhou, W., Fu, J., Yan, H., Du, X., Wang, Y., & Zhou, H. (2023). Event-triggered approximate optimal path-following control for unmanned surface vehicles with state constraints. *IEEE Transactions on Neural Networks and Learning Systems*, *34*(1), 104–118.

Zhu, C., Huang, B., Lu, Y., Li, X., & Su, Y. (2022). Distributed affine formation maneuver control of autonomous surface vehicles with event-triggered data transmission mechanism. *IEEE Transactions on Control Systems Technology*, *31*(3), 1006–1017.

Wentao Wu received his Ph.D. degree from Shanghai Jiao Tong University, Shanghai, China, 2025. From January to November 2024, he was a Visiting Research Scholar at the Department of Mechanical Engineering, University of Victoria, BC, Canada. He is currently a Postdoctoral Fellow in the Department of Aeronautical and Aviation Engineering, The Hong Kong Polytechnic University, Hong Kong, China.

His current research interests include distributed control, safety-critical control, game theory, and their applications in marine vehicles. Dr. Wu was selected for the inaugural Doctoral Special Program of Young Elite Scientist Sponsorship Program by China Association for Science and Technology (CAST) in 2025. He serves as an active reviewer of many international journals.

Lei Xu received the Ph.D. degree in mechanical engineering from the University of Victoria, Victoria, BC, Canada, in 2025. He is currently a Postdoctoral Researcher with the School of Electrical Engineering and Computer Science, KTH Royal Institute of Technology, Stockholm, Sweden.

His research interests include distributed optimization, networked control systems, event-triggered control, and Markovian jump systems.

Ruonan Liu received the B.S., M.S. and Ph.D. degrees from Xi'an Jiaotong University, Xi'an, China, in 2013, 2015 and 2019, respectively. She was a postdoctoral researcher with the School of Computer Science, Carnegie Mellon University in 2019, as well as an Alexander von Humboldt Fellow with the University of Duisburg–Essen, Germany from 2022 to 2024. She currently is an associate professor in the Department of Automation, Shanghai Jiao Tong University, and also serves as the Chair of IEEE Reliability society Shanghai Chapter.

Her research interests include condition monitoring, environment perception and autonomous decision of intelligent systems. She has been awarded the 2021 Outstanding Paper Award by IEEE Transactions on Industrial Informatics, the Runner-up Paper Award in IJCAI-W 2024, the Best Paper Award Finalist in IEEE ARM 2024, the Best Paper Award in RCAE 2024, two Best Paper Award Finalists in IROS 2025, the New Generation Star Project in IROS 2025 and recognized as one of the World's Top 2% Scientists by Stanford University consecutively from 2021 to now and selected in the Young Elite Scientist Sponsorship Program by CAST in 2022.

Weidong Zhang received his BS, MS, and Ph.D. degrees from Zhejiang University, China, in 1990, 1993, and 1996, respectively, and then worked as a Postdoctoral Fellow at Shanghai Jiao Tong University. He joined Shanghai Jiao Tong University in 1998 as an Associate Professor and has been a Full Professor since 1999. From 2003 to 2004 he worked at the University of Stuttgart, Germany, as an Alexander von Humboldt Fellow. From 2007 to 2008 he worked at Princeton University, USA, as a Visiting Professor. From 2013 to 2017 he serviced as Deputy Dean of the Department of Automation, Shanghai Jiao Tong University. He serving as a part-time professor at Hainan University from 2021. He is currently Chair Professor of Shanghai Jiao Tong University, Director of the Engineering Research Center of Marine Automation, Shanghai Municipal Education Commission, China.

His research interests include control theory, machine learning theory, and their applications in industry and robots. He is the author of more than 300 papers and 2 books. His papers have been cited for more than 23k times in Google, and he is recognized as Elsevier Most Cited Researcher and Highly Ranked Scholar-Lifetime in the Specialties of Sensor fusion, Control theory by ScholarGPS.